Compaction in the Groningen Gas Field

Suzanne Hangx

Utrecht University

Datum July 2023

Editors Jan van Elk

General Introduction

At the High Pressure and Temperature Laboratory in the Department of Earth Sciences (Faculty of Geosciences) at Utrecht University a large experimental program into compaction and movement along faults during earthquakes in Groningen was executed. The research program funded by NAM started in 2014 and lasted until 2018 (Ref. 1 to 4), when the DEEPnl project led by NWO took over (Ref. 5 to 7). Additional experiments were performed at the Shell laboratory in Amsterdam and the ExxonMobil URC laboratory in Houston.

Initially, the experiments were performed using core material obtained from the Stedum-2 well drilled in 1965 before pressure depletion in the North of the field had started. In 2015, an additional core was recovered from the newly drilled well Zeerijp-2A.

The experiments on compaction in the Groningen gas field have been documented in numerous papers published in reputable peer-reviewed journals and dissertations (Ref. 8 to 26). The current report provides an overview of the full research program into compaction performed as part of the NAM-led research program and the continuation of this program as part of the DEEPnl research program led by NWO.

Preparation of an overview report on compaction in the Groningen field was part of the 'Study Plan seismicity Groningen during pressure equilibration period' (Ref. 27) requested by SodM. This study aims to investigate the development of seismicity after close-in of the gas field, during the period of pressure equilibration. Focus is on processes that could potentially cause a delay in the decline of the seismicity in the Groningen field.

References

1. Study and Data Acquisition Plan Induced Seismicity in Groningen for the update of the Winningsplan 2016, NAM, Jan van Elk & Dirk Doornhof, December 2014.
2. Study and Data Acquisition Plan Induced Seismicity in Groningen - Update Post-Winningsplan 2016 (Part 1), NAM, Jan van Elk and Dirk Doornhof, April 2016.
3. Study and Data Acquisition Plan – 2019, NAM, Jan van Elk and Dirk Doornhof, Januari 2020.
4. Study and Data Acquisition Plan Induced Seismicity Groningen - Part 2: Subsurface Discovery Process, NAM, Jan van Elk and Dirk Doornhof, September 2020.
5. DeepNl: het contract tussen NWO en NAM, NWO and NAM, 1 oktober 2017.
6. Eerste Addendum op: Overeenkomst ten behoeve van de uitvoering van onafhankelijk wetenschappelijk onderzoek DEEPnl, NWO and NAM, January 2020.
7. Tweede Addendum op: Overeenkomst ten behoeve van de uitvoering van onafhankelijk wetenschappelijk onderzoek DEEPnlNWO and NAM, May 2023.
8. Buijze, L. (2020), Numerical and experimental simulation of fault reactivation and earthquake rupture applied to induced seismicity in the Groningen gas field, PhD thesis, 304 pp, Utrecht University, Utrecht, The Netherlands.
9. Cuesta Cano, A., J. F. Van Stappen, T. K. T. Wolterbeek, and S. J. T. Hangx (2021), Uniaxial compaction of sand using 4D X-ray tomography: The effect of mineralogy on grain-scale compaction mechanisms, Materials Today Communications, 26, 101881, doi:https://doi.org/10.1016/j.mtcomm.2020.101881.
10. Jefferd, M. A., S. J. T. Hangx, and C. J. Spiers (in prep.), The effect of loading rate and loading history on deformation of the reservoir sandstone of the Groningen Gas Field.
11. Hol, S., A. van der Linden, S. Bierman, F. Marcelis, and A. H. Makurat (2018), Rock Physical Controls on Production-induced Compaction in the Groningen Field, Scientific Reports, 8(1), 7156, doi:10.1038/s41598-018-25455-z.
12. Mehranpour, M. H., S. J. T. Hangx, and C. J. Spiers (2021), Compaction of the Groningen Gas Reservoir Sandstone: Discrete Element Modeling Using Microphysically Based Grain-Scale Interaction Laws, Journal of Geophysical Research: Solid Earth, 126(9), e2021JB021722, doi:https://doi.org/10.1029/2021JB021722.
13. Pijnenburg, R. P. J. (2019), Deformation Behavior of Reservoir Sandstones from the Seismogenic Groningen Gas Field: An experimental and mechanistic study, PhD thesis, 293 pp, Utrecht University, Utrecht.
14. Pijnenburg, R. P. J., and C. J. Spiers (2020), Microphysics of Inelastic Deformation in Reservoir Sandstones from the Seismogenic Center of the Groningen Gas Field, Rock Mechanics and Rock Engineering, doi:10.1007/s00603-020-02215-y.
15. Pijnenburg, R. P. J., B. A. Verberne, S. J. T. Hangx, and C. J. Spiers (2018), Deformation Behavior of Sandstones From the Seismogenic Groningen Gas Field: Role of Inelastic Versus Elastic Mechanisms, Journal of Geophysical Research: Solid Earth, 123(7), 5532-5558, doi:10.1029/2018jb015673.
16. Pijnenburg, R. P. J., B. A. Verberne, S. J. T. Hangx, and C. J. Spiers (2019a), Inelastic Deformation of the Slochteren Sandstone: Stress-Strain Relations and Implications for Induced Seismicity in the Groningen Gas Field, Journal of Geophysical Research: Solid Earth, 124(5), 5254-5282, doi:10.1029/2019jb017366.

17. Pijnenburg, R. P. J., B. A. Verberne, S. J. T. Hangx, and C. J. Spiers (2019b), Intergranular Clay Films Control Inelastic Deformation in the Groningen Gas Reservoir: Evidence From Split-Cylinder Deformation Tests, Journal of Geophysical Research: Solid Earth, 124(12), 12679-12702, doi:10.1029/2019jb018702.
18. Spiers, C. J., S. J. T. Hangx, and A. R. Niemeijer (2017), New approaches in experimental research on rock and fault behaviour in the Groningen gas field, Netherlands Journal of Geosciences, 96(5), s55-s69, doi:10.1017/njg.2017.32.
19. Van Stappen, J., J. A. McBeck, B. Cordonnier, R. P. J. Pijnenburg, F. Renard, C. J. Spiers, and S. J. T. Hangx (2022), 4D Synchrotron X-ray Imaging of Grain Scale Deformation Mechanisms in a Seismogenic Gas Reservoir Sandstone During Axial Compaction, Rock Mechanics and Rock Engineering, 55(8), 4697-4715, doi:10.1007/s00603-022-02842-7.
20. Verberne, B. A., S. J. T. Hangx, R. P. J. Pijnenburg, M. F. Hamers, M. R. Drury, and C. J. Spiers (2020), Drill core from seismically active sandstone gas reservoir yields clues to internal deformation mechanisms, Geology, 49(5), 483-487, doi:10.1130/g48243.1.
21. Verberne, B. A., and C. J. Spiers (2017), A Quantitative Microstructural Investigation of Depleted and Undepleted Reservoir Sandstones, in 51st U.S. Rock Mechanics/Geomechanics Symposium, edited, American Rock Mechanics Association, San Francisco, California, USA.
22. Waldmann, S., and R. Gaupp (2016), Grain-rimming kaolinite in Permian Rotliegend reservoir rocks, Sedimentary Geology, 335, 17-33, doi:https://doi.org/10.1016/j.sedgeo.2016.01.016.
23. Mehranpour, M. H., and S. J. T. Hangx (in prep.-a), How Uncertainty in 3D In-Situ Stress Affects Reservoir Compaction Behavior: A DEM Case Study of the Groningen Gas Field.
24. Mehranpour, M. H., and S. J. T. Hangx (in prep.-b), Insight into the Mechanical Behavior of Groningen Sandstone Using Discrete Element Method: Grain Size Distribution and Mineralogy Effects.
25. Shinohara, T., and S. Hangx (2023), Inelastic strain due to slow deformation of clay-bearing porous sandstone, in 84th EAGE Annual Conference & Exhibition, edited, pp. 1-5, European Association of Geoscientists and Engineers, Vienna, Austria, doi:https://doi.org/10.3997/2214-4609.202310957.
26. Shinohara, T., S. J. T. Hangx, and C. J. Spiers (in prep.), The effect of loading rate on the deformation behavior of highly porous sandstones.
27. Study Plan seismicity Groningen during pressure equilibration period, NAM, Jan van Elk, November 2022.

NAM

Title	**Compaction in the Groningen Gas Field**	**Date**	July 2023
		Initiator	Univ. Utrecht
Autor(s)	Suzanne Hangx	**Editors**	Jan van Elk
Organisation	Utrecht University	**Organisation**	NAM
Place in the Study and Data Acquisition Plan	Study Theme: Reservoir Compaction Comment: At the High Pressure and Temperature Laboratory in the Department of Earth Sciences (Faculty of Geosciences) at Utrecht University a large experimental program into compaction and movement along faults during earthquakes in Groningen was executed. The research program funded by NAM started in 2014 and lasted until 2018, when the DEEPnl project led by NWO took over. Additional experiments were performed at the Shell laboratory in Amsterdam and the ExxonMobil URC laboratory in Houston. Initially, the experiments were performed using core material obtained from the Stedum-2 well drilled in 1965 before pressure depletion in the North of the field had started. In 2015, an additional core was recovered from the newly drilled well Zeerijp-2A. The experiments on compaction in the Groningen gas field have been documented in numerous papers published in reputable peer-reviewed journals and dissertations. The current report provides an overview of the full research program into compaction performed as part of the NAM-led research program and the continuation of this program as part of the DEEPnl research program led by NWO. Preparation of an overview report on compaction in the Groningen field was part of the 'Study Plan seismicity Groningen during pressure equilibration period' requested by SodM. This study aims to investigate the development of seismicity after close-in of the gas field, during the period of pressure equilibration. Focus is on processes that could potentially cause a delay in the decline of the seismicity in the Groningen field.		
Directly linked research	• Reservoir Pressure Depletion. • Seismicity.		
Used data	Sub-surface data and core material from the Groningen field; open-hole logs, core data, pressure data, production data etc.		
Associated organisation	Shell laboratory Amsterdam and URC laboratory Houston.		
Assurance	Research has been published in peer-reviewed journals.		

Compaction in the Groningen Gas Field

An overview of our understanding of the compaction behaviour of the Slochteren sandstone and surroundings during and after production

Suzanne Hangx

Ronald Pijnenburg

With contributions by

Mark Jefferd, Mohammed Hadi Mehranpour, Mike Sep, Takahiro Shinohara, Chris Spiers

Unrestricted report

Utrecht University

Executive summary

This report summarises the work done on understanding the physical mechanisms and mechanics governing compaction behaviour of the Slochteren sandstone, performed within a *NAM*-funded research programme (2015-2021) focussing on the behaviour during production, and within the *DeepNL* research programme (2018-present) focussing on the post-abandonment phase. In these collective studies, microstructural observations, obtained from field material (depleted and undepleted core from the Groningen Gas Field) and experimental work (conventional triaxial stress and uniaxial strain experiments), combined with experimental mechanical data, simulating stress changes during production of the Groningen Gas Field, enabled us to identify the main grain-scale deformation mechanisms operating in the Slochteren sandstone.

The Slochteren sandstone mainly consists of quartz grains, and smaller amounts of K-feldspar, with the grain-to-grain contacts frequently containing µm-thick, intergranular clay films. Experimental and microstructural work suggested that most of the compaction observed in the Slochteren sandstone developed near-instantaneously, i.e. over time-scales of hours-days. Slower experiments performed over weeks to months showed decelerating creep deformation, contributing a modest 10-20% to the inelastic strain accumulated during active loading, i.e. a 10-20% time-dependent contribution to strain. Together with the mechanistic constraints of the field, this suggests that reservoir compaction in the Groningen Gas Field is largely rate-insensitive, with only a modest contribution of time- or rate-sensitive mechanisms. During production, compaction is dominated by (virtually) rate-insensitive processes, like poro-elastic deformation, and compaction of and slip along the intergranular clay films. On longer time-scales of weeks-months, time-dependent compaction may be governed by a different mechanism, notably by stress corrosion (intragranular) cracking. To what extent even longer-term compaction behaviour (decades-centuries) will be influenced by this slow creep process, or by other creep processes such as pressure solution, still requires further investigation and quantification.

Extrapolating experimental data obtained at the slowest strain rates achievable in the lab (i.e. $10^{-8 \text{ or } -9}$ s^{-1}) to the current compaction rate in the field (i.e. 1000 slower) was attempted using various empirical rate-dependent models, such as the RTCM model. Doing so suggested that additional strains of 10-50% can be expected (i.e. inelastic strain in excess of what has already been accumulated at rapid/lab deformation rates). Though experimental work hints at excess strain in the field after abandonment likely being at the lower end of this range (10-20%), the broad range in forecasted strain illustrates the need to better constrain the models used for extrapolation to field timescales. Since such slow deformation rates cannot be accessed in the lab, understanding the microphysical processes underlying sandstone deformation is required.

Microphysical models describing rate-insensitive compaction were implemented in Discrete Element models to assess sandstone compaction behaviour at the cm-dm scale. These numerical models can be used to evaluate reservoir compaction in different locations on the field due to pressure equilibration or repressurisation, with rate-sensitive mechanisms, such as stress corrosion cracking, to be added at a later stage. However, it should be noted that even if the Slochteren reservoir formation would not exhibit much ongoing compaction after field closure due to time-dependent compaction processes, that does not necessarily imply independence of subsidence and seismicity from production rate and strategy. Even if reservoir compaction is fully time-independent, subsidence and seismicity may be influenced by time-dependent (creep) deformation of the overlying Basal Zechstein and rock salt, and by pore pressure re-equilibration within/near the reservoir (e.g. the clay-rich Ten Boer and Ameland members), and/or the underlying low-permeable (Carboniferous) shales. In addition, time dependent behaviour may perhaps be caused by transient fluid flow along faults.

Contents

1 Introduction

The Groningen Gas Field in the north of the Netherlands is one of the largest onshore gas fields in the world. However, prolonged gas production has reduced the initial gas pressure from 35 MPa in 1963 to 8 MPa by 2015. The resulting increase in effective overburden stress has led to compaction at the reservoir level. This compaction is expressed at the surface as subsidence, currently forecasted to be ~50 cm by the end of field life [*Nederlandse Aardolie Maatschappij (NAM)*, 2016]. At the same time, differential compaction across the many faults in the reservoir has led to induced seismicity, with a maximum seismic event of magnitude 3.6 in 2012 in Huizinge (see Figure 1; [*Nederlandse Aardolie Maatschappij (NAM)*, 2016]).

While purely (poro-)elastic reservoir behaviour is easily quantified and modelled, a portion of the total compaction will be inelastic [*Spiers et al.*, 2017] and may continue long after exploitation has ceased [*Ketelaar et al.*, 2011]. Since the Groningen Gas Field is heavily faulted [*Nederlandse Aardolie Maatschappij (NAM)*, 2013], lateral and vertical variations in the reservoir, controlled by the depositional environment [*Visser et al.*, 2016], would lead to differential compaction across those faults, resulting in slip and potentially induced seismicity. It has been shown that most earthquakes occur at locations where compaction, expressed as surface subsidence, has exceeded 18 cm [*Bourne et al.*, 2014]. Those locations tend be in areas where the Slochteren reservoir sandstone has a high porosity, such as in the central area of the field (cf. Figure 1a and b).

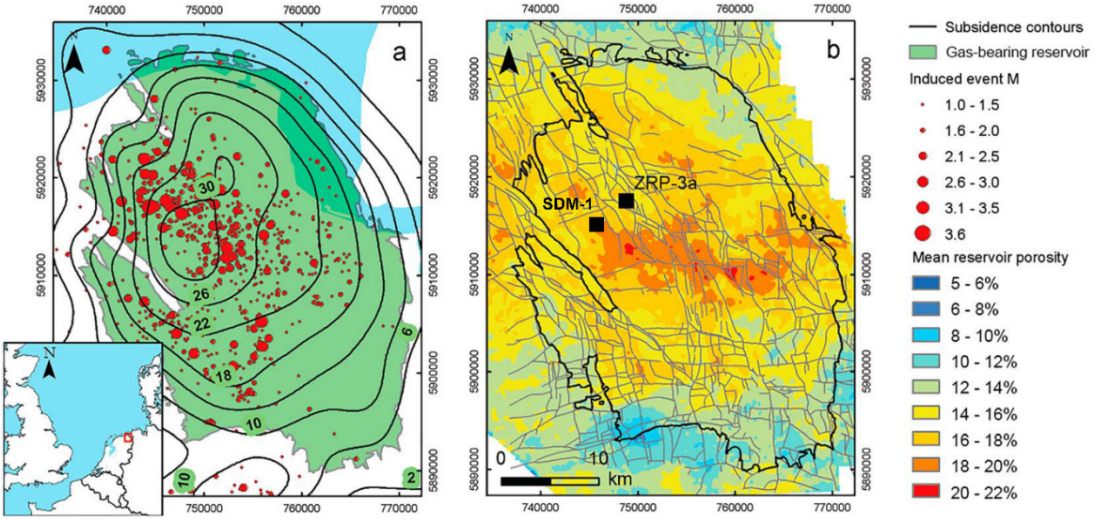

Figure 1. Maps showing (a) the location of the Groningen Gas Field, the extent of the gas-bearing reservoir at approximately 3,000-m depth, contours of the surface subsidence measured in 2013, and induced earthquake magnitudes and locations in the period 1991–2017 (www.knmi.nl - seismic catalogue), and (b) the vertically averaged porosity of the Slochteren reservoir sandstone and the main faults. Fault throws range up to 300 m [Buijze et al., 2017], thus cutting the top of the reservoir. The porosity and subsidence data were provided courtesy of the field operator [Nederlandse Aardolie Maatschappij (NAM), 2013]. This figure is modified after Pijnenburg et al. [2019a].

Compaction, subsidence and induced seismicity are predominantly controlled by mechanical deformation processes physically deforming the structure of the rock. However, the underlying chemical and physical processes operating at the grain contact-scale, controlling inelastic compaction, are poorly understood [*Brantut et al.*, 2014; *J Zhang et al.*, 1990], limiting the forecasting of permanent reservoir deformation. Relevant mechanisms could include coupled processes of intergranular sliding, contact crushing, grain-scale fracturing, sorption/desorption and/or stress-induced dissolution-precipitation reactions (pressure solution). **To evaluate the impact of gas extraction and to assess future production-related hazards, identification and quantification of the mechanisms controlling compaction of the reservoir, and its immediate over- and underburden, during production and after abandonment is required.** Only then an advanced modelling capability, based on the physical and chemical processes operating, can be developed. To achieve this, experiments need to be performed under realistic in-situ pressure-temperature-chemical conditions, simulating compaction at depth, coupled with detailed microstructural analysis and microphysical theory. This was the premise under which an extensive research programme (from 2015-2021), funded by the *Nederlandse Aardolie Maatschappij*, was established at Utrecht University to investigate Slochteren reservoir compaction during production. This programme was followed by a number of research projects, embedded in the NWO-organised *DeepNL programme* (from 2018 until now), investigating the post-abandonment behaviour of the reservoir, as well as the immediate under- and overburden formations. This report gives an overview of the main conclusions from those studies to date.

2 The Groningen Gas Field

The vast Groningen Gas Field (~30 by 30 km) is located in the NE-Netherlands (Figure 1a), with the main reservoir unit consisting of the ~100-200 m thick Slochteren reservoir sandstone, located at about 3 km depth. The gas reservoir lies unconformably on its source rock, the organic-rich Carboniferous shales. Its base consists of coarse, poorly sorted fluvial sandstones and conglomerates, gradating into cross-bedded, intermediate- to well-sorted aeolian sandstones towards the top [*Grötsch et al.*, 2011]. The top 50-150 m of the reservoir are gas-bearing, with 25±10% of the pores being filled with connate water containing ~4.4 M NaCl (25.5 wt-%) [*Waldmann*, 2012]. The reservoir is overlain by another clay-rich sequence, the 50 m thick Ten Boer claystone, followed by 500-1000 m of Permian evaporites [*Amthor and Okkerman*, 1998].

Overall, the Slochteren sandstone is quartz rich (72–90 vol%), with lesser amounts of feldspar (8–25 vol%), clay (0.5–5.5 vol%), and lithic fragments (3–10 vol%; basaltic and sedimentary lithoclasts [*Waldmann et al.*, 2014; *Waldmann and Gaupp*, 2016; *Waldmann et al.*, 2017]). The mean size of the main framework grains ranges between 150 and 250 µm [*Pijnenburg et al.*, 2018]. The surfaces of the quartz and feldspar grains are coated with thin clay films (1-10-µm thick), which are also present in many grain contacts [*Gaupp et al.*, 1993; *Waldmann and Gaupp*, 2016]. Porosity (φ_0), determined from wireline logs and fluid-immersion measurements [*Nederlandse Aardolie Maatschappij (NAM)*, 2013], indicate an average value of 18-22% at the centre of the field, decreasing to 12-16% towards the field margins (see also Figure 1b).

In 2015, to investigate the physical mechanisms and mechanics controlling compaction in the Slochteren sandstone, field operator *Nederlandse Aardolie Maatschappij BV* (NAM) launched a drilling operation at the Zeerijp ZRP-3A well (for location see Figure 1b) to retrieve reservoir core from the highly depleted, most seismogenic, central part of the field. Slochteren sandstone core recovered before depletion in 1965, from the nearby Stedum SDM-1 well (see location in Figure 1b), was used as an undeformed, pre-depletion benchmark. At the time of retrieval of the ZRP-3A core, the pressure in the field had fallen from the initial 35 MPa to a uniform 8 MPa, with subsidence reaching ~33 cm in the centre of the field. Assuming subsidence at the surface corresponds to compaction at depth, this suggests very small vertical reservoir compaction strains of 0.1-0.3%, which is consistent with in-situ fibre-optic strain measurements [*Cannon and Kole*, 2017]. Furthermore, the decrease in reservoir pore pressure resulted in an upward shift of the gas-water contact by about 12 m (i.e. ~2971 m true vertical depth [*Waldmann et al.*, 2017]). However, no significant differences in mineralogy were observed for samples from the transition zone compared to the under- and overlying rocks. Therefore, no significant water-rock interactions or mineralogical changes are expected due to formation water ingress, suggestive of a negligible or zero impact on the mechanical stability of the gas-water contact transition zone [*Waldmann et al.*, 2017].

The top of the reservoir is located at ~2900 m true vertical depth, with an average temperature of 100°C (varies from 80-120°C [*Nederlandse Aardolie Maatschappij (NAM)*, 2016]. The maximum stress (σ_1) is considered to be vertical [*Van Eijs*, 2015] and was estimated to be 65 MPa prior to gas production [*Schutjens et al.*, 1995]. The minimum horizontal stress (σ_3) was determined to be 39-43 MPa [*Breckels and van Eekelen*, 1982; *Hettema et al.*, 2000; *Van Eijs*, 2015], while the initial pore pressure (P_p) was 35 MPa [*Nederlandse Aardolie Maatschappij (NAM)*, 2016; *Schutjens et al.*, 1995]. This suggests that the pre-production state of stress consisted of a maximum principal effective stress ($\sigma_1^{eff} = \sigma_1 - P_p$) of 30 MPa, a minimum principal effective stress ($\sigma_3^{eff} = \sigma_3 - P_p$) of 4-8 MPa, and a differential stress $Q = (\sigma_1 - \sigma_3)$ of 22-26 MPa. Current pore pressure in the field ranges from 7-17 MPa, with 10 MPa at the Zeerijp-2 well [*Nederlandse Aardolie Maatschappij (NAM)*, 2019], which would suggest that, assuming the overburden stress remains constant, σ_1^{eff} = 55 MPa and at most σ_3^{eff} = 29-33 MPa (with $(\sigma_1 - \sigma_3)$ = 22-26 MPa), depending on the field stress path. These estimated changes in $(\sigma_1 - \sigma_3)$ and σ_3^{eff} provided the basis for our choice of loading paths in the experiments described in the below sections.

3 Field observations

To improve the in-situ compaction monitoring program in the Groningen Gas Field, the newly drilled ZRP-3A well was equipped with real-time compaction measurement equipment using a Discrete Strain Sensing (DSS) system. Two separate DSS cables were installed along ~450 m of the well, spanning the base of the Zechstein formation down to the top of the Carboniferous shales [*Cannon and Kole*, 2017]. The first period of DSS monitoring started on 12/10/2015 and lasted a little over a year, showing that strain was inhomogeneously distributed along the well but mainly compressive and increasing with time (Figure 2). Most of the in-situ measured compaction occurred in the Slochteren reservoir itself, though significant compaction was also measured in the

overlying Ten Boer claystone and the top of the underlying Carboniferous shales, suggesting time-dependent compaction in the over- and underburden is also contributing to subsidence and movements along pre-existing faults.

Though the total in-situ strains in the reservoir that have accumulated since production started are estimated to be small (0.1-0.3%), core taken from the ZRP-3A well was compared to the undeformed material from the nearby SDM-1 well to see if there was evidence for the inelastic deformation mechanisms controlling reservoir compaction. Potential mechanisms of inelastic reservoir compaction included (1) fracture of grains forming the load-supporting rock framework, (2) grain-scale dissolution-precipitation, and (3) processes operating within grain contacts, like asperity crushing/dissolution, clay film deformation and slip [*Spiers et al.*, 2017; *Verberne et al.*, 2020]. Lithological variations, characterizing the central part of the field, were sampled and inspected using techniques ranging from visual inspection to optical and backscattered electron (BSE) microscopy, X-ray mapping, cathodoluminescence (CL) imaging, electron backscatter diffraction (EBSD) mapping, and image analysis.

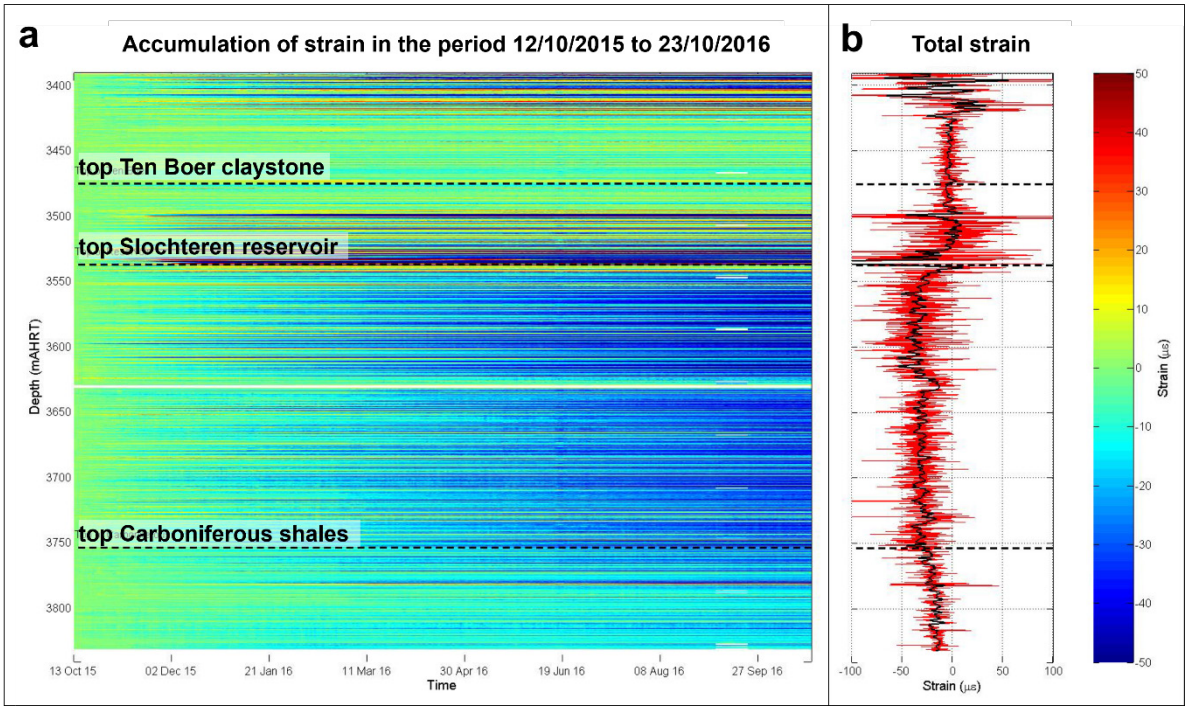

Figure 2. (a) Strain measured along the DSS cable during the first year of monitoring (12/10/2015 – 23/10/2016). Note that the dashed lines indicate the tops of the various lithological units, as indicated. (b) Total strain along the cable measured on 23/10/2016. The black curve represents a heavily smoothed version of the data to aid in visualization of the average. Modified after Cannon and Kole [2017].

Depleted (ZRP-3A), undepleted (SDM-1) and lab-deformed (SDM-1; simulating depletion, deformed up to 0.2% inelastic strain) sandstone samples were found to be indistinguishable at hand-specimen scale. Quantitative microstructural analysis of 28 thin sections, taken from 15-20 m-spaced depth intervals of both cores, was performed [*Verberne et al.*, 2020; *Verberne and Spiers*, 2017]. No evidence was found for more, or more recent, diffusive mass transport in depleted versus undepleted samples, nor for statistically significant differences in the reactivation of healed fractures. Furthermore, EBSD mapping of Dauphiné twin boundaries showed that (simulated) depletion was insufficient to measurably enhance Dauphiné twinning. Crack density analysis showed that total crack densities were indistinguishable between depleted and undepleted material, as well as lab-deformed sandstone. This suggests that grain failure did not play a significant role in producing inelastic strain as a result of gas production. However, when focusing on specific mineral phases, it was found that K-feldspar grain were preferentially cracked compared with quartz and other minerals in the depleted core material. Given the low abundance of K-feldspars compared with quartz (~15%), and their spatially scattered distribution in the reservoir rock, feldspar grains likely acted as passive markers indicative of deformation of the surrounding grain framework, without significantly contributing to permanent deformation.

At the same time, weak clay films coating many of the detrital grain contacts play a role here as well. Long-term clay consolidation strongly depends on effective normal stress [*Brown et al.*, 2017]. Since the Groningen Gas Field lies close to its maximum burial depth [*Gaupp and Okkerman*, 2011], intergranular clay films compacted during burial would almost certainly deform further as the effective vertical stress increased from ~30 to ~55 MPa during depletion of the Groningen reservoir. Inelastic compaction of individual, 2–5-µm-thick intergranular clay films [*Waldmann et al.*, 2017] by 4% (i.e. 0.1–0.2 µm) would already lead to reservoir compaction of 0.1-0.2% strain for typical grain sizes of 100-200 µm [*Pijnenburg et al.*, 2019b]. Given the in-situ boundary condition of 1-D vertical strain (zero lateral strain), such clay film compaction would need to be coupled with intergranular sliding (clay film shearing).

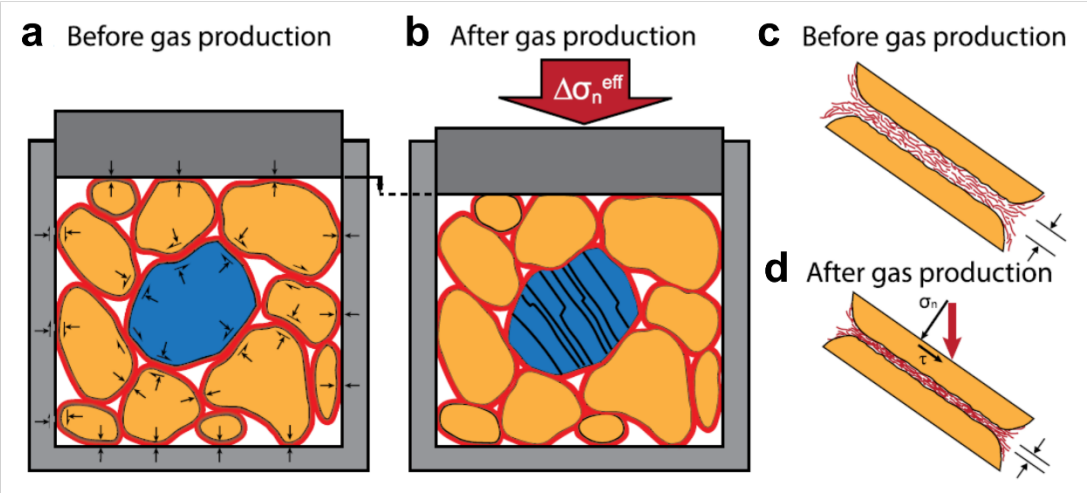

Figure 3. Schematic diagram illustrating inferred reservoir compaction mechanism. Note, in this simplification, all grain surfaces are coated with uniform clay films. In a real sandstone reservoir, clay films are discontinuous and locally absent, especially in distal regions of the field. (a, b) Idealized volume of reservoir sandstone undergoing uniaxial compaction strain path typical of producing gas reservoirs. Orange: load-supporting quartz framework; blue: sparse feldspar grains; red: clay films. Normal and shear displacements are indicated at selected grain contacts. (c, d) Deformation at grain-contact scale. Increase in vertical effective stress ($\Delta\sigma_{n,eff}$) due to pore-pressure depletion leads to uniaxial compaction of bulk rock (a → b), accommodated by elastic deformation of quartz grain framework plus compaction and shear of clay films trapped in load-bearing grain contacts (c → d). Increased stresses driving clay film deformation lead to fracture of weaker, corroded K-feldspar grains (b), while stronger quartz grains remain intact. Shear within clay-filled grain contacts leads to increased lateral stresses due to zero lateral strain. Taken from Verberne et al. [2020].

Therefore, it is inferred that elastic deformation of the Slochteren sandstone, coupled with inelastic deformation by intergranular clay film compression and shear, offers the most viable explanation for the strains recorded by cracked feldspars in the depleted core (see Figure 3 for a schematic diagram [*Verberne et al.*, 2020]). It should be noted that while these compaction strains match field subsidence and in-situ strain data well, they are virtually impossible to detect in the post-mortem microstructure, as there are no internal strain markers either at the grain or clay film scales. However, in-situ, timelapse micro X-ray tomography (micro-XCT) imaging of loose quartz aggregates, with and without K-feldspar and clay simulating the Slochteren sandstone composition, confirmed that the suggested mechanism is possible, with clay films dampening quartz grain breakage, while K-feldspar grains act as markers evidencing deformation of the load-bearing framework [*Cuesta Cano et al.*, 2021].

4 Experimental approaches

To systematically identify and quantify the grain-scale mechanisms controlling compaction in the Slochteren sandstone during production (main focus of the *NAM* research program; Section 5) and after abandonment (main focus of the *DeepNL*-related projects; Section 6) triaxial deformation experiments, coupled with detailed microstructural analysis, were performed. It should be noted that experimental studies based on conventional deformation tests express the mechanical behaviour in terms of mean effective stress ($P = [\sigma_1 + \sigma_2 + \sigma_3]/3$ - pore pressure P_p) versus total porosity reduction ($\Delta\varphi_t$), as illustrated in Figure 4. Typically, P-$\Delta\varphi_t$ curves exhibit a transition from initial, nonlinear, concave-up behaviour (i.e. Stage 1 behaviour) to near-linear behaviour (i.e. Stage 2 behaviour), which in turn is followed by nonlinear behaviour. The nonlinear behaviour is characterised by dilation at low P and φ (i.e. Stage 3d, with suffix 'd' for dilation) and by nonlinear compaction at high P and φ (Stage 3c, with suffix 'c' for compaction).

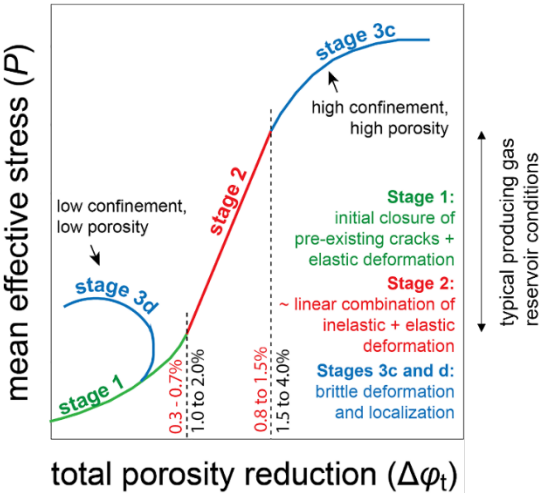

Figure 4. Schematic diagram showing the different stages in mean effective stress (P) versus total porosity reduction ($\Delta\varphi_t$) behavior typically seen in mechanical tests on sandstones. Note the effects of confining pressure and porosity on Stage 3 behavior (dilation = suffix "d" versus compaction = "c"). Typical values of total axial strain (red) and total porosity reduction (black), measured at the end of each stage are indicated. Note that typical reservoir conditions, representative for gas production, typically fall within Stage 2 of the P- $\Delta\varphi_t$ curve. Modified after Pijnenburg et al. [2019b].

Stage 1 behaviour is generally believed to represent poro-elastic deformation, combined with semi-recoverable closure of pre-existing damage or cracks [*David et al.*, 2012; *Walsh*, 1965], and typically persists up to $\Delta\varphi_t$ values of ~0.3% at low-effective confining pressures (P_c^{eff} = confining pressure $P_c - P_p$ and at low φ) to 2.0% (high P_c^{eff}, high φ). At low P_c^{eff} (i.e. $P_c^{eff} < 20$ MPa), Stage 1 transitions directly into Stage 3d at $\Delta\varphi_t \approx 0.3\%$. By contrast, at $P_c^{eff} > 20$ MPa, Stage 1 is followed by Stage 2 behaviour. Recent experimental studies have shown that the near-linear behaviour seen in Stage 2, persisting up to 1.5-4.0% $\Delta\varphi_t$, reflects combined elastic and inelastic behaviour, where the inelastic part constitutes some 20% to 70% of the total deformation [*Bernabé et al.*, 1994; *Hol et al.*, 2015a; *Hol et al.*, 2018; *Pijnenburg et al.*, 2018]. Eventually Stage 2 behaviour gives way to Stage 3c (nonlinear compaction). Both Stages 3c and 3d are accompanied by pervasive intragranular cracking and intergranular or interparticle shear, frequently localizing in shear fractures (Stage 3d), or compaction bands (Stage 3c [*Baud et al.*, 2004; *Fortin et al.*, 2005; *Tembe et al.*, 2008; *Wu et al.*, 2000]). This shows that it is clear that inelastic deformation contributes significantly to the compressive deformation of sandstone at the small strains (< 1%) relevant for producing reservoirs. Therefore, the work done within the *NAM* and *DeepNL* research programmes has largely focussed on understanding Stage 2 inelastic behaviour.

In total, four different types of deformation experiments were performed, which can be briefly described as:

1. **Conventional triaxial deformation experiments on Slochteren sandstone of 12-25% porosity**, at constant strain rates of ~ 10^{-5} s^{-1} (i.e. 10^7 times faster than the in-situ field strain rate of 10^{-12} s^{-1}), exploring the full deformation behaviour of the Slochteren sandstone [*Pijnenburg et al.*, 2018] – Section 5.1.
2. **Time-lapse conventional triaxial compression experiments on Slochteren sandstone** aimed at visualizing deformation using high-resolution electron microscopy [*Pijnenburg et al.*, 2019b] or synchrotron micro XCT [*Van Stappen et al.*, 2022] – Section 5.1.
3. **Conventional triaxial and uniaxial (zero lateral displacement) deformation experiments at strain rates of 10^{-3} to 10^{-9} s^{-1}** on highly porous Slochteren sandstone [*Pijnenburg*, 2019; *Shinohara and Hangx*, 2023] and analogue sandstone [*Shinohara et al.*, in prep.] to evaluate the effect of deformation rate on compaction and the controlling deformation mechanism after abandonment – Section 6.1. Note that conventional triaxial experiments are the more commonly performed type of experiments, where the material is allowed to deform in both the axial and radial direction. Uniaxial strain, or zero lateral displacement, experiments are more difficult to perform but allow for a more realistic simulation of in-situ conditions, as radial deformation is constrained.
4. **Cyclic triaxial experiments** on Slochteren sandstone and analogue sandstone to investigate the effect of loading rate and loading history on compaction, in the context of repressurisation of the reservoir [*Jefferd et al.*, in prep.] – Section 6.2.

When possible, Slochteren sandstone, obtained from the ZRP-3A and SDM-1 cores, was used for the experiments. However, when using core material, the number of 25-mm-diameter samples with similar initial properties (i.e. from the same depth interval) is limited to about five due to the ~10 cm core radius. In cyclic triaxial experiments (experiment type 4) and some of the experiments described under point 3, it was deemed useful to have more than five samples readily available, with similar starting properties. Therefore, for these studies (i.e.

[*Shinohara et al.*, in prep.] and [*Jefferd et al.*, in prep.]), samples were obtained from analogous, outcropping sandstone. The selected analogue sandstone (Bleurswiller sandstone, Vosges [*Baud et al.*, 2015]) is similar in mineralogical composition, porosity and mechanical behaviour to highly porous Slochteren material (φ_0 = 21%). All experiments were performed under realistic in-situ temperature, pressure and chemical conditions, at the stress state prevailing in the reservoir (T = 100°C, 4 M NaCl brine at 10 MPa pore pressure; effective stress conditions, see Section 2). To complement the clay-bearing, highly porous Bleurswiller sandstone, the quartz-rich Bentheimer sandstone (> 95% quartz, φ_0 = 23%) was selected as a clay-free counterpart to evaluate the influence of intergranular clay films on slow, time-dependent compaction behaviour.

5 Compaction during gas production

5.1 Time-independent deformation of the Slochteren sandstone

The time-independent (instantaneous) deformation behaviour of Slochteren sandstone was explored through deviatoric (triaxial) and hydrostatic load-cycling experiments [*Pijnenburg et al.*, 2019a]. The deformation behaviour was explored using ZRP-3A samples having initial porosity (φ_0) values of 13.4 to 26.4%, at strain rates of ~10^{-5} s^{-1} (experiment duration of several hours), and for P_c^{eff} values up to 320 MPa and differential stresses up to 135 MPa, chosen to cover and exceed the stresses relevant for reservoir compaction in Groningen. The results are shown in Figure 5 and show similar mean effective stress (P = [σ_1 + σ_2 + σ_3]/3 - P_p) versus total porosity reduction ($\Delta\varphi_t$) behaviour to that typically reported for sandstone (Figure 4).

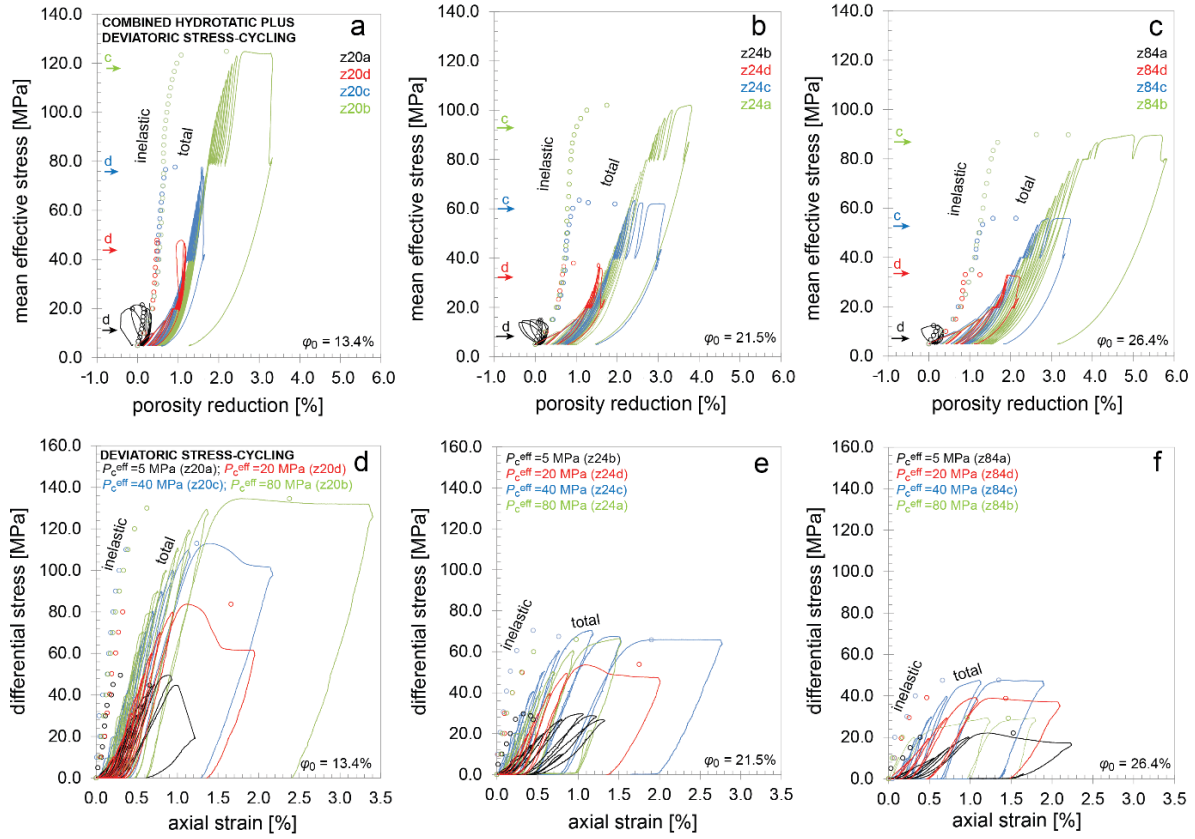

Figure 5. Plots showing the mechanical data obtained in our combined hydrostatic plus deviatoric stress-cycling experiments performed on Slochteren sandstone samples from the ZRP-3A well, having low (φ_0 = 13.4%; left column), intermediate (φ_0 = 21.5%; middle column) and high initial porosities (φ_0 = 26.4%; right column). All experiments consisted of hydrostatic stress cycling up to effective confining pressures of 5, 20, 40, and 80 MPa, followed by deviatoric stress cycling at constant P_c^{eff}. (a–c) Mean effective stress versus total ($\Delta\varphi_t$; solid curves) and inelastic porosity reduction data ($\Delta\varphi_i$; open circles). (d–f) Plots showing differential stress (σ_1 - σ_3) versus total (ε_t; solid curves) and inelastic axial strain (ε_i; open circles) data. Arrows and annotations "d" and "c" indicate the onset of Stages 3d or 3c, respectively. Note that an inelastic contribution to strain was measured after each stress cycle and observed even in Stage 2. Taken from Pijnenburg et al. [2019a].

During the near-linear portion of P - $\Delta\varphi_t$ behaviour (i.e. Stage 2; see Figure 4), which is often taken to be fully poroelastic, 30 to 50% of the total axial strain and porosity reduction measured was found to be inelastic. This near-linear behaviour, and the associated small elastic plus inelastic strains ($\varepsilon \leq 1\%$) were judged to be most

relevant to producing reservoirs, such as the Groningen Gas Field and smaller gas fields in the Netherlands. Subsequent microstructural analyses of the deformed samples suggested that the inelastic deformation developing within Stage 2 was largely accommodated by intergranular displacements, with intragranular cracking becoming increasingly important towards higher strains (Stage 3), and particularly where non-linear, dilatant (onset marked by "d" in Figure 5a-c) or compactive behaviour (onset marked by "c" in Figure 5a-c) was observed.

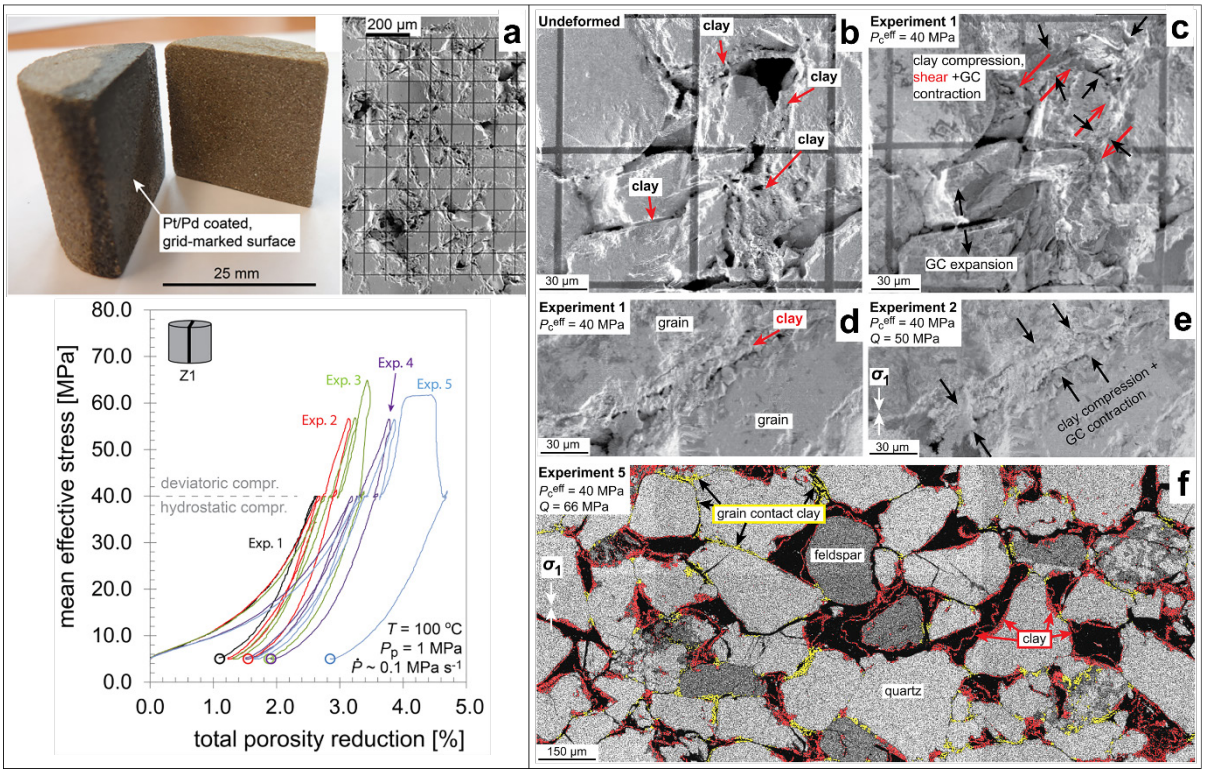

Figure 6: Micrographs obtained in successive experiments performed on (a) a single split-cylinder sample containing a reference grid on the split surface. The P- $\Delta\varphi_t$ plot shows the different experiment stages at which images of the deformed grid were taken. (b-e) Before and after test images, highlighting the intergranular clays and their role played in accommodating inelastic strain during Experiments 1 and 2, in which Stages 1 and 2 were explored (see Figure 4). (f) Electron dispersive X-ray spectrometry image obtained after the final Experiment 5. Pore-filling/coating clays are mapped in red, while clays present within grain contacts are shown in yellow. Modified after Pijnenburg et al. [2019b].

To further elucidate the mechanisms enabling intergranular displacements at small strains, *Pijnenburg et al.* [2019b] performed a sequence of five stress/strain-cycling plus strain-marker-imaging experiments on a single split-cylinder sample (φ_0 = 20.4%) of Slochteren sandstone (Figure 6a). The tests were performed under in-situ conditions of effective confining pressure (P_c^{eff} = 40 MPa) and temperature (100°C), exploring increasingly larger differential stresses (up to 75 MPa) and/or axial strains (up to 4.8%) in consecutive runs (Figure 6b). Control tests confirmed no mechanical effects of the split-cylinder approach, compared to an intact sample. At smaller, reservoir-relevant strains (≤ 1%), inelastic deformation was largely accommodated by slip on and consolidation of µm-thick clay films present within grain boundaries, with a smaller role played by intragranular cracking (Figure 6b-e; in line with inferred mechanisms observed in field core [*Verberne et al.*, 2020]). In addition, an EDX map showing the clay films present within grain contacts, filling pores, and coating pore walls is given in Figure 6f. Intergranular deformations again appear to be larger in or near grain boundaries filled with clay films, which are present throughout the ZRP-3A material (see yellow clay films indicated in Figure 6f). At higher axial strains (> 1.4%, i.e. in Stage 3), the split-cylinder method revealed pervasive intragranular cracking plus intergranular shear displacements within localised, conjugate bands, as seen in previous experiments on material with similar porosity at similar effective stresses [*Pijnenburg et al.*, 2019b]. By this stage, the observed permanent grain-scale displacements were larger (several microns, that is, > 1-3% strain). Using a simplified sandstone model, it was shown that at constant effective stresses corresponding to the current state of depletion in the Groningen field (σ_1^{eff} = 57 MPa, σ_3^{eff} = 27 MPa) deformation by clay consolidation plus intergranular slip is rapid (order: mm/s), hence virtually time- or rate-insensitive at the time-scales pertaining to the field. This was furthermore confirmed through time-lapse synchrotron micro XCT imaging of a deforming Slochteren sandstone sample. In this experiment imaging small-strain deformation in real time, compaction occurred through grain rearrangement accommodated

by intergranular slip and normal displacements across grain boundaries, in particular, by closure of open grain boundaries or compaction of inter-granular clay films [*Van Stappen et al.*, 2022].

5.2 Modelling compaction during gas production

The above mentioned experimental results and microstructural observations formed the basis to develop relationships to realistically and accurately describe the mechanical behaviour of the Slochteren sandstone observed during production. As a first start, an empirical model was developed to describe the mechanical data obtained by [*Pijnenburg et al.*, 2019a]. The subsequent microstructural observations [*Pijnenburg et al.*, 2019b] formed the basis to deriving a constitutive model describing the real microphysical behaviour of the material. Eventually, this constitutive model was implemented in a numerical approach, the Discrete Element Method (DEM), used to model the behaviour of granular packs. This DE model aimed to simulate compaction of the reservoir in space and time, including variations in porosity, mineralogy, grain size (distribution) and even stress state. We developed a new particle-interaction law (contact model) for classic DEM to explicitly account for the experimentally observed mechanisms of nonlinear elasticity, intergranular clay film deformation, and grain breakage, thereby populating the model with realistic grain-scale mechanisms [*Mehranpour et al.*, 2021].

5.2.1 An empirical model for inelastic plus elastic deformation behavior of Slochteren sandstone

At the small strains relevant to depletion in the Groningen field ($\varepsilon \leq 1\%$; cf. Stage 2, Figure 4), the inelastic deformation response measured in stress-cycling experiments (Figure 6) was shown to be isotropic and well-described by an empirical, Cam-clay-type plasticity model (model outlined in *Pijnenburg et al.* [2019a]). This plasticity model was combined with a poroeleastic model to also describe the elastic contribution. The model was first tested through a comparison of the mechanical behaviour implied by the model for 1-D compaction (zero lateral strain) with data obtained in pore pressure depletion experiments conducted under uniaxial strain boundary conditions, obtained on Slochteren sandstone samples from the ZRP-3A well by *Hol et al.* [2018], i.e. from the same core as used in the present study (Figure 7).

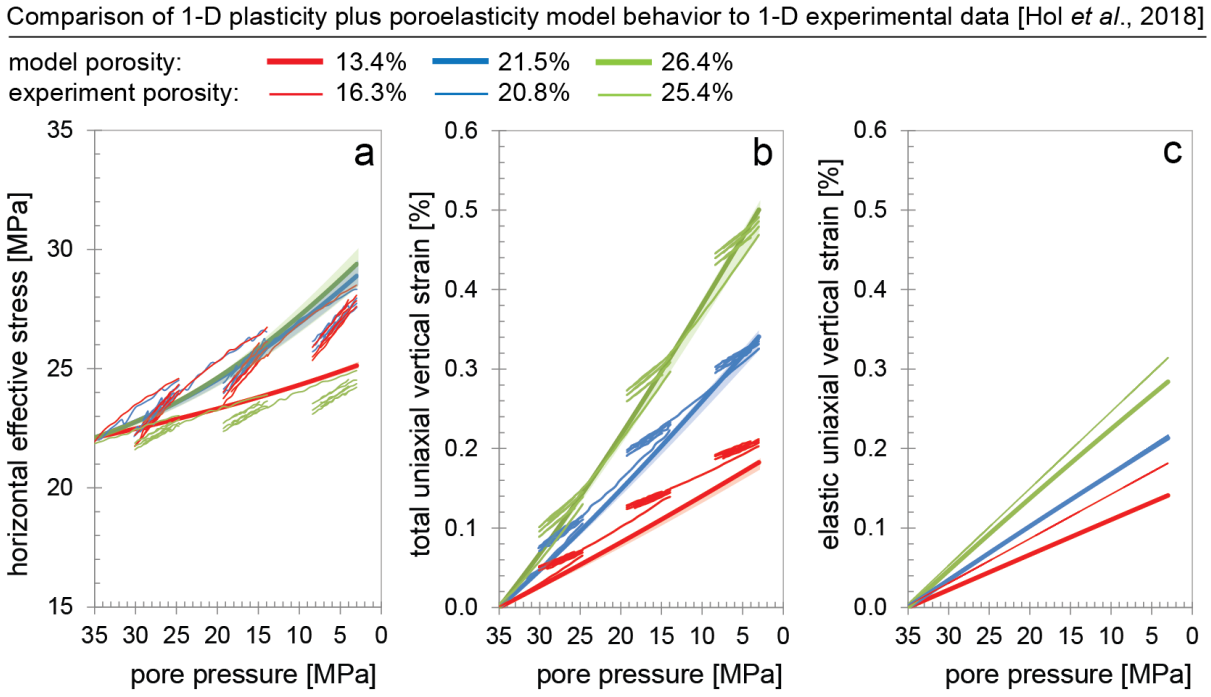

Figure 7. Comparison between the 1-D (uniaxial strain) behaviour implied by the plasticity plus poroelasticity model reported by Pijnenburg et al. [2019a], and the data obtained in the 1-D cyclic pore pressure depletion experiments performed on Slochteren sandstone by Hol et al. [2018], on samples with similar initial porosity (φ_0). Figure taken from Chapter 6 of Pijnenburg [2019].

Comparison demonstrated a broad agreement between the model and the experimental results obtained by *Hol et al.* [2018], as shown in Figure 7. Based on this, it was inferred that the present empirical model adequately described the elastic plus (near-instantaneous) inelastic compaction behaviour of Slochteren sandstone under the 1-D boundary conditions expected in the bulk of the Groningen reservoir. Hence the model is likely applicable more generally, such as for small 3-D deformations in the neighbourhood of faults.

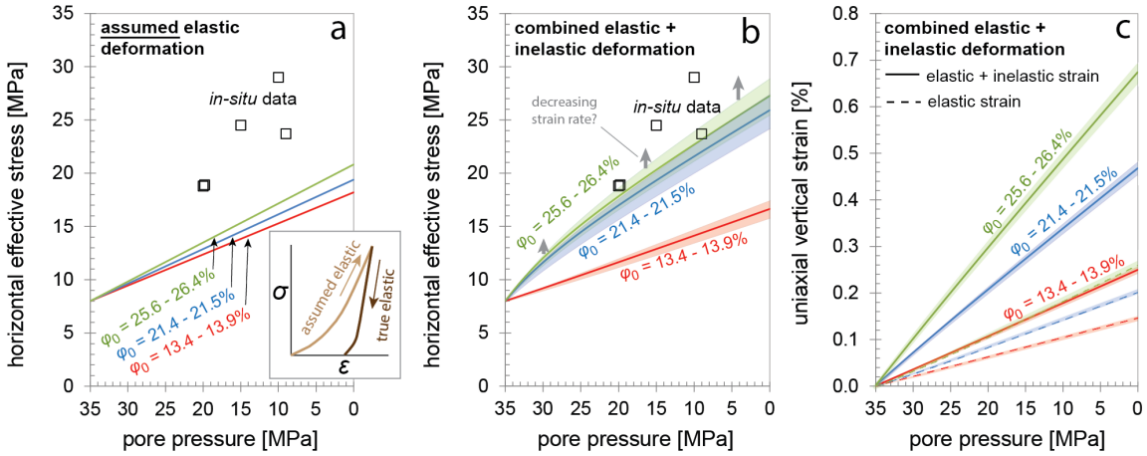

Figure 8. Plots showing the effect of the inelastic contribution to compaction of Slochteren on predicted effective horizontal stress (σ_3^{eff}) changes and elastic versus inelastic strain partitioning during pore pressure reduction under uniaxial strain conditions, expected to be prevalent in the Groningen field. Taken from Pijnenburg et al. [2019a].

The plasticity plus poroelasticity model was then applied to predict the inelastic versus elastic, 1-D (i.e. uniaxial) compaction behaviour expected to accompany depletion of the Groningen reservoir. It was shown that again 30 to 50% of the total uniaxial strain accrued is inelastic (Figure 8c). This means that a similar proportion of the total mechanical work input into the reservoir during depletion is dissipated and unavailable for seismic release. It further implies that poroelastic reservoir compaction models significantly overestimate the energy budget available in the reservoir for seismicity. The impact of this on the magnitude-frequency distribution of earthquakes in Groningen requires further investigation, following the lead given for example by *Bourne et al.* [2014]. Furthermore, it is demonstrated that by accounting for the inelastic contribution to compaction, the measured in-situ horizontal stress evolution during pore pressure reduction is much better reproduced (correspondence within 25% - Figure 8b), compared to purely poroelastic estimates (correspondence within 25 to 50% - Figure 8a). Geomechanical modelling of compaction and fault rupture in the Groningen Gas Field has so far assumed elastic reservoir behaviour [*Bourne et al.*, 2014; *Dempsey and Suckale*, 2017; *Lele et al.*, 2016; *Smith et al.*, 2019; *Van Eijs et al.*, 2006; *Wassing et al.*, 2016; *Zbinden et al.*, 2017]. The present findings demonstrated that including the inelastic contribution to reservoir compaction has a key role to play in future geomechanical modelling, and in understanding induced seismicity. However, to what extent the current, essentially time-independent, plasticity plus poro-elasticity model, calibrated to the data obtained in the above laboratory experiments (hours in duration) applies at the much longer, decade time-scales relevant to production of the Groningen field is as yet unclear, and formed the focus of some of the work done within the subsequent *DeepNL programme*.

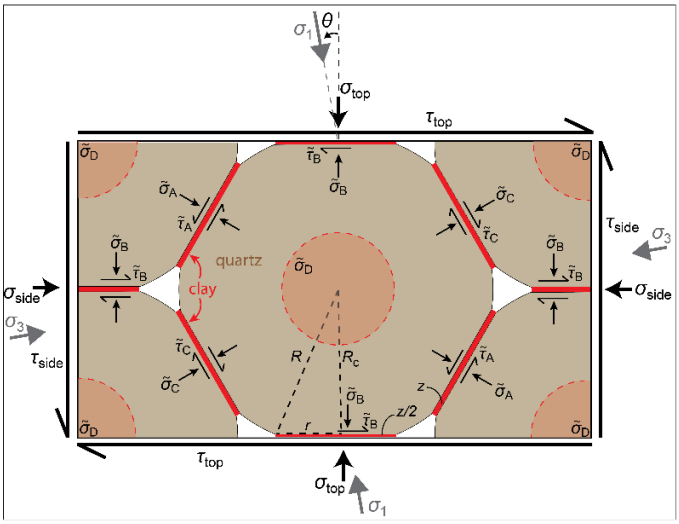

Figure 9. Model microstructure assumed by Pijnenburg and Spiers [2020], for inelastic deformation of the clay-bearing Slochteren sandstone undergoing triaxial compression. The microstructure constitutes a simple hexagonal pack of quasi-spherical quartz grains with flattened contacts, each covered with illite clay films (indicated red). The maximum vertical stress (σ_1) acts at an angle θ to the top of the unit cell, implying (external) normal and shear stresses on the top (σ_{top}, τ_{top}) and side (σ_{side}, τ_{side}) of the unit cell. These external stresses imply normal ($\tilde{\sigma}$) and shear stresses ($\tilde{\tau}$) on grain contacts, which, if sufficiently large, may cause consolidation of- and/or slip on the intergranular clay (thickness z), and/or cracking of the quartz grains. Further details are provided in Pijnenburg and Spiers [2020].

5.2.2 *Microphysical model for intergranular clay compaction and slip*

Based on microstructural analyses (cf. Section 5.1), Pijnenburg and Spiers [2020] developed a simplified microphysical model, incorporating intergranular clay deformation and grain failure. They used this model to assess the extent to which these mechanisms could account for the instantaneous (time-independent) inelastic deformation behaviour seen in the experiments on Slochteren sandstones. The model assumes a regular pack of quasi-spherical quartz grains with truncated grain contacts, each covered with µm-thick clay films (Figure 9).

Comparison of model predictions of the deformation behaviour with the experimental data showed broad agreement [*Pijnenburg and Spiers*, 2020]. At the small strains relevant to producing reservoirs (i.e. where $\varepsilon \leq 1\%$), the inelastic deformation could be largely accounted for by consolidation of and slip on intergranular clay films, while the higher strain behaviour exceeding that relevant to reservoirs was well-captured by assuming dilatant intergranular slip and intragranular cracking. Since grain boundary clay film consolidation and slip were found to be time- or rate-insensitive deformation processes at stresses pertaining to the depletion of the Groningen reservoir, reservoir compaction by these mechanisms is also expected to be time- or rate-insensitive. In accordance with this, long-term compaction experiments were performed on the Slochteren sandstone over weeks [*Pijnenburg et al.*, 2018] to months [*Hol et al.*, 2015a] at similar stresses, temperature (100 °C), and chemical conditions (4M NaCl brine) to those seen in the Groningen Gas Field. These experiments showed that the bulk of Stage 2 inelastic compaction has been virtually instantaneous, while decelerating creep deformation contributed a modest 10 to 20% to the inelastic strain accumulated during active loading. The time-independent plasticity plus poro-elasticity model outlined by *Pijnenburg et al.* [2019a] therefore captured the main trends of the in-situ compaction behaviour at the decade time-scales relevant to the field, though compaction strains and lateral stresses may be slightly underestimated by 10 to 20% due to other (decelerating) creep effects seen in long-term (weeks-months) experiments [*Hol et al.*, 2015a; *Pijnenburg et al.*, 2018]. To constrain the long-term (decades - centuries) behaviour of the reservoir, time-dependent mechanisms, such as stress corrosion cracking or other slow creep processes (e.g. pressure solution), typically not seen in lab experiments of conventional (hours/days) duration, need to be quantified and included in the constitutive model.

5.2.3 *A Discrete Element Model including the new Slochteren Sandstone Contact Model*

Discrete Element Method (DEM) is a powerful numerical method aimed at linking grain-scale properties to macro-mechanical behaviour of granular media [*Marketos and Bolton*, 2009]. As such, it may be an appropriate tool for predicting sandstone behaviour. To date, DEM simulations have proven to be able to qualitatively describe stress-strain behaviour of granular aggregates, mainly through fitting to specific experimental data sets. However, typically used contact models assume (visco-)elastic and frictional interactions at the grain-to-grain contacts. Therefore, current DEM simulations are unable to capture the effects of intergranular clay film deformation, or of grain crushing and pore collapse resulting from microcracking, in a realistic manner as seen in cemented sandstones like the Slochteren sandstone. To improve the predictive capability of DEM simulations for sandstones

under reservoir conditions, a new contact model describing both nonlinear elastic and inelastic interactions, resulting from compaction of and slip along intergranular clay films [*Pijnenburg et al.*, 2019b] was incorporated in DEM (Itasca's Particle Flow Code, PFC (see *Potyondy and Cundall* [2004], *Mehranpour et al.* [2021]). In addition, grain failure was included on the basis of a grain indentation model leading to the propagation of a penny-shaped microfractures.

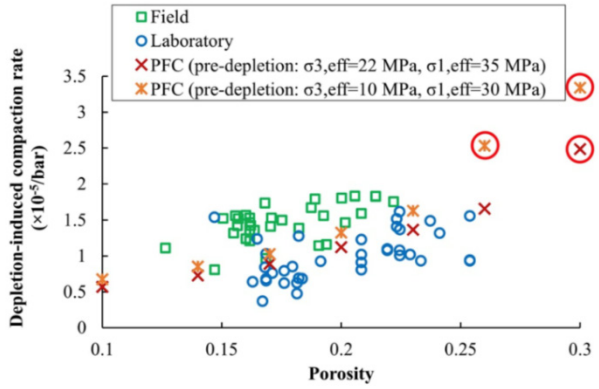

Figure 10. Depletion-induced compaction rates (amount of strain per bar pore pressure depletion) as a function of porosity obtained from uniaxial compaction experiments (blue circles; Hol et al. [2018]) and numerical simulations (red and orange crosses; this study), as well as from in-situ field data (green squares; Cannon and Kole [2017]). Note that the simulation predictions are performed for two different initial stress conditions: red crosses, initial stress conditions as employed by Hol et al. [2018]; and orange crosses, slightly lower initial effective stress conditions, taking into account measurement uncertainty. Simulations undergoing pervasive grain failure prior to reaching the maximum axial stress, leading to breakdown of the model, are indicated with a large red circle. Figure taken from Mehranpour et al. [2021].

In the new Slochteren Sandstone Contact Model (SSCM), it was assumed that particles representing the quartz grain framework were unbonded, meaning that the intergranular clay layers were assumed to have negligible cohesion in both tension and shear. In addition, sand grains were allowed to deform elastically, as well as display irreversible consolidation and shear of the intergranular clay films and quartz grain failure, in line with experimental observations [*Pijnenburg et al.*, 2019a; b]. The SSC model was calibrated against a limited set of hydrostatic and deviatoric loading data obtained in conventional triaxial compression tests performed on the Slochteren sandstone (by *Pijnenburg et al.* [2019a]). The model was further validated by simulating independent pore pressure experiments conducted under in-situ reservoir stress and uniaxial strain conditions [*Hol et al.*, 2018], as well as measured in-situ compaction [*Cannon and Kole*, 2017], as shown in Figure 10.

Overall, the SSC model showed good agreement between the experimental data and the simulations, though significant grain breakage was predicted to occur in highly porous, modelled samples (>20% porosity) at effective axial stresses of > 60 MPa. Furthermore, predicted depletion-induced compaction rates, expressed as the amount of strain per bar of pore pressure depletion, are slightly higher than the average laboratory rates, though they fall in the same range and show a similar dependence on porosity. By contrast, simulations also showed that the predicted compaction rates fell at the lower limit of the field-measured depletion-induced compaction rate. This discrepancy is inferred to be due to the short period of in-situ field data collection, uncertainties in average porosity over the field measurement interval, and/or uncertainties in the in-situ state of stress.

After calibration and validation of the model, it was used to systematically investigate the compaction behaviour of Slochteren sandstone with different porosities, particle size distributions, and clay contents, as well as a wider range of stress-strain boundary conditions. As such, the SSC model makes it possible to study the mechanical behaviour of a single, "digital", sample under numerous boundary conditions and loading paths. This offers potential to better constrain in-situ stresses and compaction behaviour throughout the field, at least at the cm-dm scale. Furthermore, this capability allows for the generation of a data bank suitable for fitting analytical constitutive models to the simulated data to obtain strain hardening deformation laws and macroscopic yield/failure criteria for sandstones, which can be used for upscaling to the reservoir scale.

5.2.4 Effects of mineralogy, grain size distribution and horizontal stress on compaction: DEM simulations

Within the *DeepNL* research programme, the SSC model developed in the *NAM*-funded programme was further utilised to systematically investigate the effects of mineralogy (% K-feldspar, presence/absence of intergranular clay films), mean grain size and grain size distribution, and stress path on the compaction behaviour of the simulated Slochteren sandstone [*Mehranpour and Hangx*, in prep.-a; b]. This allowed for assessment of sandstone compaction behaviour in a broad range of scenarios, relevant for the Groningen Gas Field.

Petrographical studies have shown that, while intergranular clay films are prevalent in the centre of the field [*Waldmann et al.*, 2017], with a clear south-to-north trend of increasing grain-coating clay content [*Visser*, 2016].

At the same time, given the depositional environment of the area, average grain sizes and grain size distributions also vary throughout the field [*Visser et al.*, 2016]. Therefore, in these series of simulations, on the one hand the K-feldspar content (0, 5, 10 and 15%; random distribution) was systematically varied for aggregates with and without intergranular clay films. Similar to the field and experimental observations, the K-feldspar grains could serve as passive markers for deformation of the load-bearing quartz framework [*Mehranpour and Hangx*, in prep.-b]. On the other hand, grain size distributions were varied from normal to Gaussian (based on volume or counting fraction), with ranges of 110-300 µm (narrow) and 60-350 µm (broad) [*Mehranpour and Hangx*, in prep.-b]. All simulations on the simulated quartz aggregates were performed under the same stress conditions: 1) triaxial compression at an effective horizontal stress of 20 MPa until yield or failure occurred, and 2) pore pressure depletion under zero lateral strain boundary conditions (uniaxial compression) similar to the stress path of the Groningen Gas Field up to full depletion [*Hol et al.*, 2018; *Mehranpour et al.*, 2021].

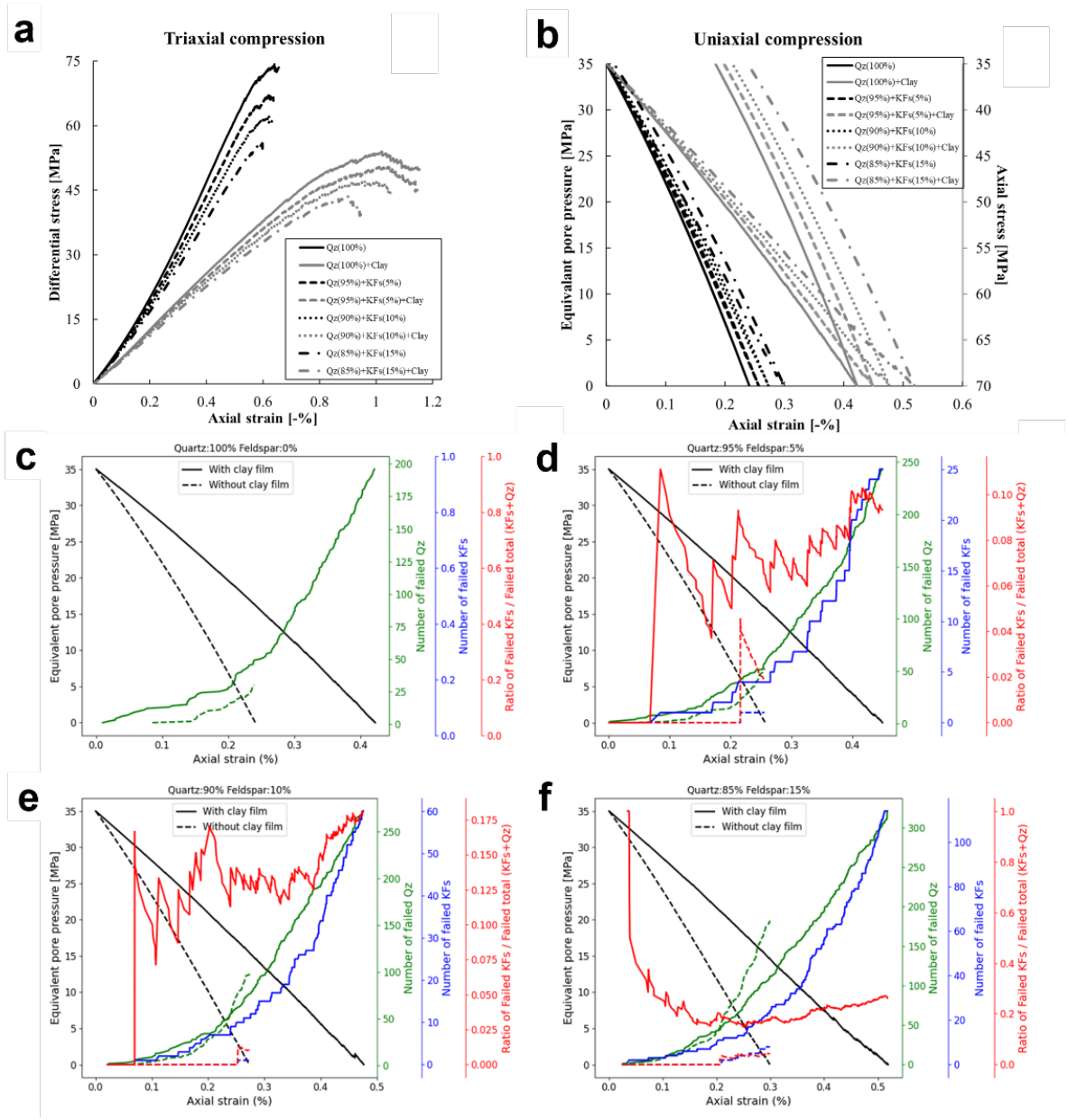

Figure 11. Simulated compaction behavior of aggregates with a porosity of 21.5% and a range of K-feldspar ratio (0, 5, 10 and 15%) and clay film thickness under (a) triaxial compression with a lateral stress of 20 MPa, and (b) cyclic uniaxial compression with an initial confining stress similar to the Groningen gas reservoir pre-depletion stress state (σ_3^{eff}= 20 MPa) and 35 MPa axial stress cycle range, simulating reservoir depletion to full depletion and repressurisation. (c-f) The number of failed grains (quartz: green; K-feldspar: blue), as well as the fraction of failed K-feldspar grains (red lines) in the uniaxial compaction simulations shown in (b), for K-feldspar contents of (c) zero %, (d) 5%, (e) 10% and (f) 15%. Solid lines: aggregates with intergranular clay films; dashed lines: clay-free aggregates. Figure adapted from Mehranpour and Hangx [in prep.-b].

For an aggregate of 21.5% porosity, with a uniform grain size distribution and grain size range of 110-300 µm deformed under triaxial loading conditions, the strength and elastic modulus of simulated Slochteren sandstone decreased when increasing the K-feldspar content from zero to 15% (Figure 11a-b), likely as K-feldspar contains cleavage planes, may be corroded, and hence tends to be weaker than quartz [*Hangx et al.*, 2010] thus exhibiting increased fracturing (see Figure 11c-f, cf. quartz vs. K-feldspar breakage). Furthermore, the presence of thin clay films in the grain contacts led to additional strain (compare solid and dashed lines in Figure 11a), which was in part due to the compaction of and slip along these clay films, together with increased brittle fracturing of both quartz and K-feldspar grains. Similar behaviour was seen when the simulated aggregates were deformed along the stress path expected for full depletion of the field, with more total and permanent strain accumulated in aggregates with clay films and higher K-feldspar content (Figure 11b). Overall, increasing K-feldspar content and including intergranular clay films led to more breakage of the quartz and K-feldspar grains, with K-feldspar showing preferential breakage, especially for less corroded, stiffer grains (Figure 11c-f), as also seen in the high porosity, depleted core material retrieved from the field [*Verberne et al.*, 2020]. It was inferred that in the absence of clay films, more of the stress is carried by the stronger, load-bearing quartz framework, protecting the weaker K-feldspar grains from breakage. In turn, with fewer K-feldspar grains breaking, there would be less stress arching around quartz grains in their vicinity, further reducing the possibility to accumulate strain [*Mehranpour and Hangx*, in prep.-b]. It should be noted that selected simulations on aggregates (90% quartz, 10% K-feldspar) showed that the extent of grain breakage also scaled with porosity, as expected, with fewer grains breaking in lower porosity material.

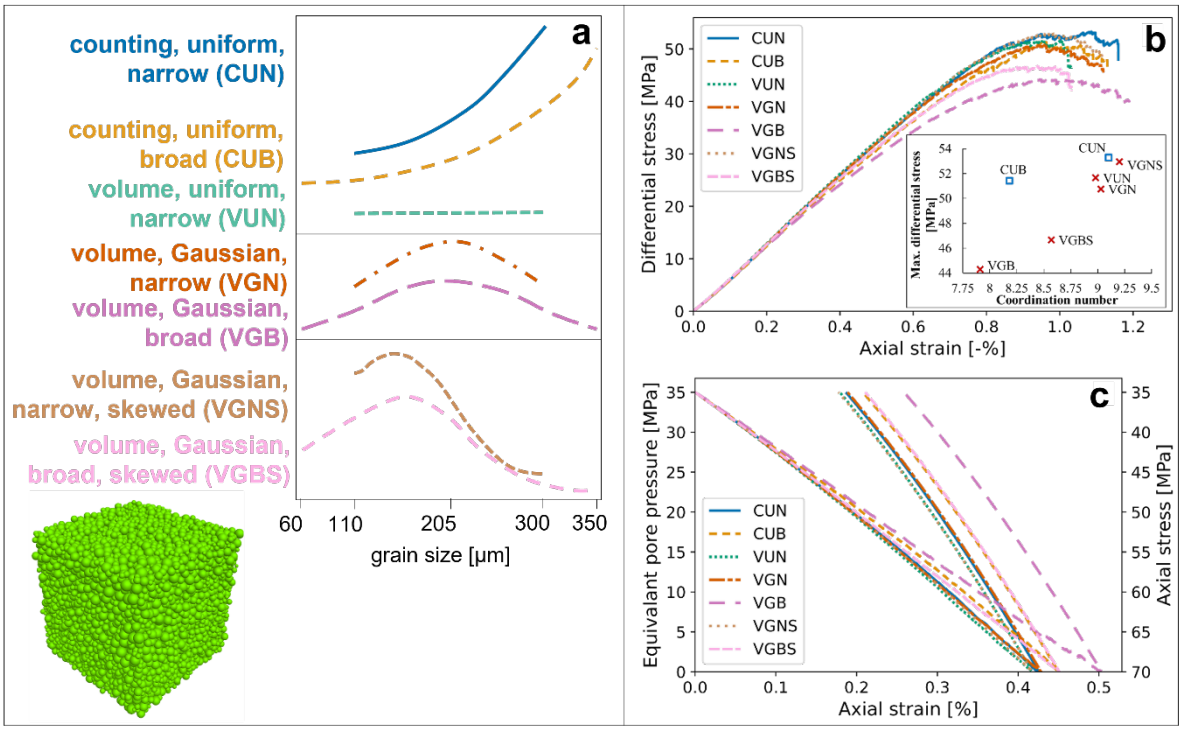

Figure 12. a) Schematic diagram showing the grain size distributions investigated in DEM simulations, either as counting (i.e. number of grains) or volume fraction distributions. Simulated compaction behaviour of simulated pure quartz aggregates with a porosity of 21.5% and a range of grain size distribution (GSD) under (b) triaxial compression with a lateral stress of 20 MPa (insert: maximum differential stress versus the average coordination number for each GSD), and (c) cyclic uniaxial compression with an initial confining stress similar to the Groningen gas reservoir pre-depletion stress state (σ_3^{eff}= 20 MPa) and 35 MPa axial stress cycle range, simulating reservoir depletion to full depletion and repressurisation. Figure modified after Mehranpour and Hangx [in prep.-a].

For a pure quartz aggregate of 21.5% porosity, deformed under the same triaxial and uniaxial stress conditions, grain size distribution (see Figure 12a for selected distributions) simulations showed a significant impact on the extent of compaction (Figure 12b-c). Aggregates with a narrow grain size distribution (i.e. 110-300 µm) typically displayed higher failure strengths, as well as less total and permanent strain, compared to their broader grain size distribution counterparts (cf. CUN, VUN and VGN vs. CUB and VBG; Figure 12b-c). It should be noted that broad grain size distributions skewed to contain a larger fine-sized fraction also showed higher peak strengths and less compaction than their non-skewed counterparts (cf. VGBS vs. VGB; Figure 12b-c). Likely the finer particles

dampened the stress concentrations on the larger grains, leading to less breakage of the larger grains, as also observed in loose sand aggregates [*Hangx and Brantut*, 2019]. The simulations performed to date demonstrate the potential DEM, including realistic grain contact behaviour, has to generate a database for predicted compaction behaviour of Slochteren sandstone, taking into account lateral and horizontal variations in mineralogy, porosity and grain size (distribution).

For three pure quartz aggregates with porosities of 13.4% (130-330 μm grain size), 21.5% (110-300 μm grain size) and 26.4% (150-390 μm grain size), based on previously studied sample material [*Hol et al.*, 2018], simulations were performed under different boundary conditions aimed to study the impact of the state of stress [*Mehranpour and Hangx*, in prep.-a]. For simulated uniaxial compression conditions, similar to the stress path of the Groningen Gas Field, simulations suggested that for the highest porosity sandstone, failure accompanied by substantial compaction is achieved during gas production, which would mean that the perceived in-situ state of stress is not the true stress state. Polyaxial simulations, taking into account both the minimum and maximum horizontal stress, suggested that the pre-production intermediate principal stress tends to have a bigger effect on the compaction behaviour than expected, especially at low minimum principal stress values. As such, it is predicted that it is likely that the pre-production minimum horizontal stress was higher than 10 MPa, in order for the high porosity zones to be able to bear the state of stress. From the simulations, it was inferred that the minimum horizontal stress was probably ~15 MPa prior to production, with the maximum horizontal stress being on the order of 15-20 MPa, i.e. a horizontal stress ratio of ~1-1.3, in line with field observations [*Van Eijs*, 2015].

6 Compaction in the reservoir after abandonment of the field: insights from recent studies

As shown in Section 5.1, deformation of the Slochteren sandstone during production is controlled by both elastic and time-independent, inelastic mechanisms. This work already hinted at time- or rate-dependent compaction playing a modest role on the longer term. This led to continued research, focussing on elucidating these possible time-dependent mechanisms, as after abandonment of the field, when gas pressure remains virtually constant, they may play an increasing role in controlling inelastic compaction of the reservoir. Such mechanisms could include stress corrosion cracking (i.e. time-dependent crack growth aided by the presence of fluids), pressure solution (i.e. stress-induced dissolution and precipitation, potentially enhanced by the presence of intergranular clay films), or other yet unidentified mechanisms. However, at present it is unclear which mechanism(s) will control post-abandonment compaction behaviour (> 10-100 years), and if there will be a gradual transition from one mechanism to another over time. Therefore, in the framework of the *DeepNL programme*, dedicated experiments and analyses were performed to explore the microphysical processes operating at the grain contacts, particularly at very slow loading rates, contributing to inelastic strain (Section 6.1 [*Shinohara et al.*, in prep.]).

At the same time, after abandonment, pressure equilibration throughout the field [*Nederlandse Aardolie Maatschappij (NAM)*, 2021], and re-pressurisation aided by inflow of the surrounding aquifer [*Wildenborg et al.*, 2022], may lead to further deformation of the reservoir. The former may lead to additional compaction, particularly in the northern regions of the field that have been experienced less pressure reduction during production [*Nederlandse Aardolie Maatschappij (NAM)*, 2021]. By contrast, the latter will reduce the effective state of stress again and may lead to (partial) recovery of elastic compaction. Systematic experiments were performed to investigate the effect of loading history on subsequent inelastic strain (Section 6.2 [*Jefferd et al.*, in prep.]).

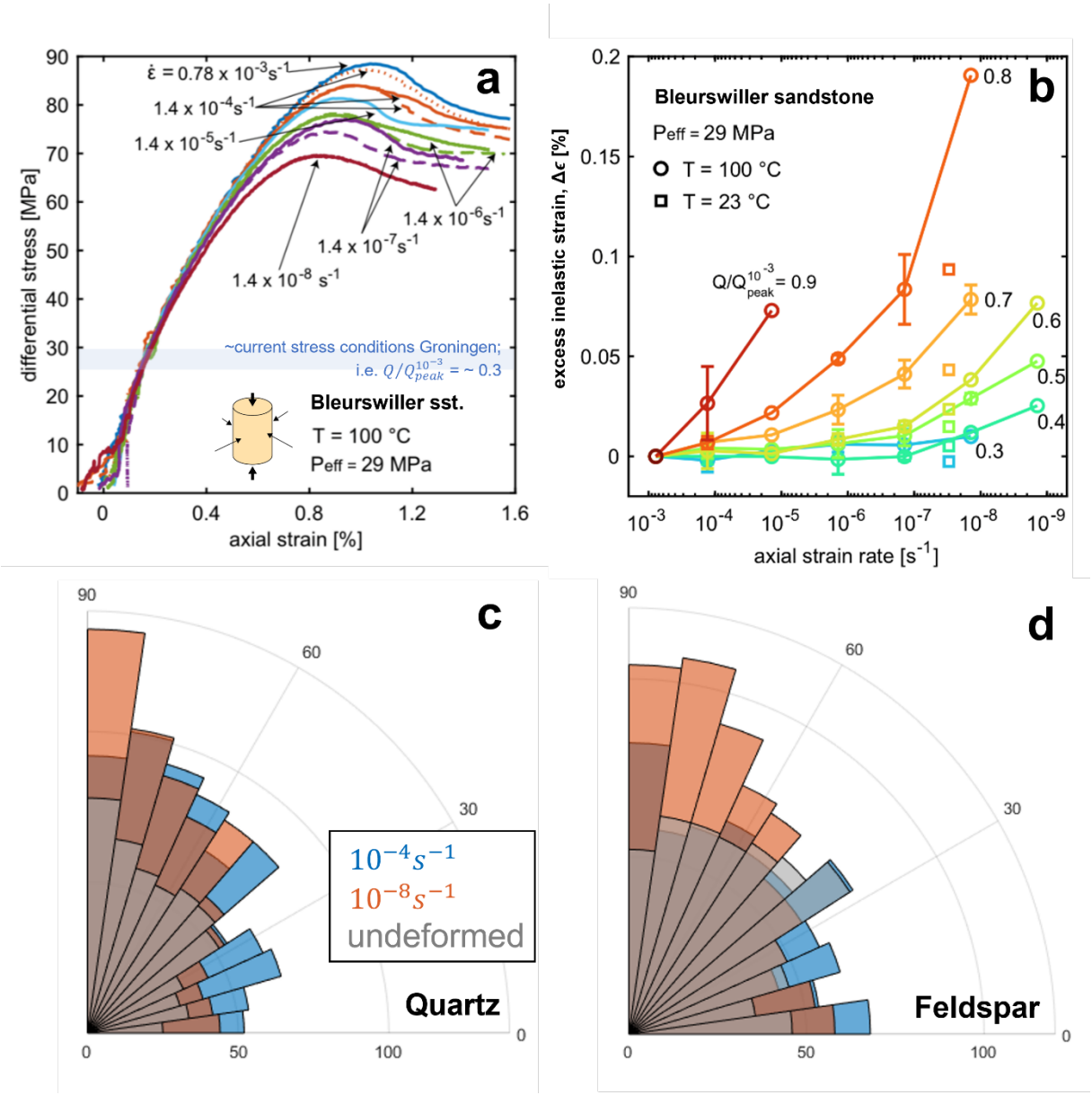

Figure 13. (a) Mechanical data obtained in conventional triaxial loading experiments performed on water-saturated Bleurswiller sandstone shown as differential stress ($Q = \sigma_1 - \sigma_3$) versus total axial strain (ε_{tot}) data, obtained at different axial strain rates at 100°C and 29 MPa effective confining pressure. (b) Excess inelastic strain as a function of axial strain rate at various differential stress levels that ranges from 30 to 90% of peak differential stress reached at an axial strain rate of 10^{-3} s^{-1} (Q/Q_{peak} 10^{-3}). Error bars show standard deviation. Crack counts and crack orientations are shown for (c) quartz (n_{undef} = 545, $n_{10\text{-}4}$ = 821, $n_{10\text{-}8}$ = 772) and (d) feldspar grains (n_{undef} = 619, $n_{10\text{-}4}$ = 707, $n_{10\text{-}8}$ = 773), in deformed and undeformed samples, where n denotes the number of counted cracks. Note that a crack orientation of 90° means that the cracks are oriented parallel to the loading direction. Figure modified after Shinohara et al. [in prep.].

6.1 Time-dependent grain-scale mechanisms operating in the Slochteren reservoir

6.1.1 Slow crack growth in load-bearing grains

To elucidate the time-dependent mechanism(s) that could contribute to sandstone compaction after abandonment, *conventional triaxial* experiments were performed to systematically investigate the effect of loading strain rate (strain rates of 10^{-3}-10^{-9} s^{-1}) on the elastic vs. inelastic compaction of water-saturated sandstone [*Shinohara et al.*, in prep.]. Given the limited availability of Slochteren sandstone samples with similar properties (max. five samples per depth interval of any core), these experiments were performed on analogue sandstone, consisting of the clay-bearing Bleurswiller sandstone (cf. Section 4), as well as quartz-rich Bentheimer sandstone, as a clay-free counterpart. Results showed a systematic lowering of the stress-strain curves with decreasing axial strain rate (i.e. slower loading rate) in both sandstones (see Figure 13a for the Bleurswiller sandstone). In contrast to the quartz-rich Bentheimer sandstone, the Bleurswiller sandstone also showed more compaction at lower strain

rates at lower differential stress values (< 70% peak differential stress, i.e. conditions relevant for sandstone reservoirs). Assuming the experiments performed at rapid loading rates (i.e. 10^{-3} s^{-1}, experiment time of several seconds) showed very little time-dependent deformation, it is possible to calculate the excess inelastic strain obtained at a slower rate for a given differential stress, i.e. $\Delta\epsilon$ = ϵ(at slower rate) - ϵ(at $\dot{\epsilon}$ 10^{-3} s^{-1}) at a given $Q/Q_{peak}^{10\text{-}3}$ (Figure 13b). At the stress conditions relevant for the Groningen Gas Field (see blue bar in Figure 13), this $Q/Q_{peak}^{10\text{-}3} \approx 0.3$. The results obtained on the Bleurswiller sandstone, suggest that under those conditions, decelerating strain rate from 10^{-3} s^{-1} to 10^{-9} s^{-1} leads to approximately a 10% increase in inelastic strain, in line with observations made previously (see Section 5.1 [*Hol et al.*, 2015a; *Pijnenburg et al.*, 2018]).

The observed dependence of the deformation behaviour on temperature, confining pressure and pore fluid pH, plus detailed microstructural analysis, gives insight in the main grain-scale deformation mechanism. It is inferred that for the Bleurswiller sandstone, at lower differential stress (< 70% peak differential stress), the observed rate effect is mainly caused by intergranular clay compaction and slip, coupled with grain breakage to accommodate further displacements. It should be noted that at slower deformation rates, crack orientations were largely aligned parallel to the loading direction, compared to more randomly oriented cracks at faster rates (Figure 13c-d). For both the Bleurswiller and Bentheimer sandstone, stress corrosion cracking coupled with intergranular sliding dominated compaction at higher differential stress, as is also often seen in other studies performed at near-failure stress conditions [*Baud et al.*, 2015; *Wong et al.*, 2001].

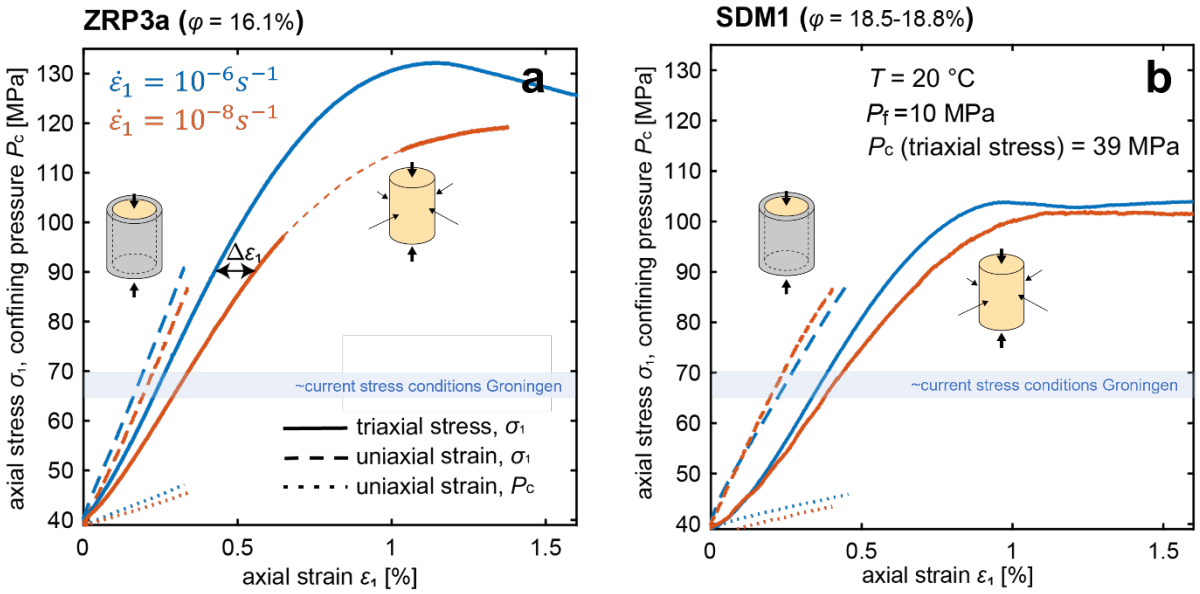

Figure 14. Mechanical data obtained in conventional triaxial stress (solid lines) and uniaxial strain (dashed lines) experiments on water-saturated Slochteren sandstone, performed at room temperature and strains rates of 10^{-6} and 10^{-8} s^{-1} (blue and red curves, respectively). Applied axial stress σ_1 (solid and dashed curves) and confining pressure P_c (dotted curves, for uniaxial experiments only) versus total axial strain for (a) material obtained from the Zeerijp-3A well with a porosity of 16.1%, and (b) material obtained from the Stedum-1 well with a porosity of 18.5-18.8%. Note that in (a), due to technical issues, part of the data obtained in the triaxial experiment performed at axial strain rate of $10^{-8}s^{-1}$ is missing. The missing part is shown with a small-dash, interpolated, curve. Figure modified after Shinohara and Hangx [2023] and currently unpublished data.

For a select set of Slochteren sandstone samples (φ_0 = 16.1-18.8%) both *conventional triaxial and uniaxial compression experiments* were performed to verify if the behaviour observed for the analogue sandstone was representative for the Slochteren material (Figure 14 [*Shinohara and Hangx*, 2023]). The triaxial experiments displayed similar behaviour as observed for Bleurswiller sandstone, with a lowering of the peak stress and more excess strain developing in the slower loading rate experiments (see solid curves in Figure 14). This behaviour was also observed in cyclic loading experiments on Slochteren sandstone under the same conditions, with varying loading rates between cycles [*Jefferd et al.*, in prep.]. By contrast, the uniaxial experiments appeared to be hardly impacted by the loading rate and display substantially less axial strain, in line with previous observations on Slochteren sandstone [*Hol et al.*, 2018]. The increase in confining pressure required to inhibit the sample from expanding laterally was carefully monitored in the uniaxial experiments (see dotted lines in Figure 14). Confining pressure (P_c^{eff} (initial) = 39 MPa) needed to be increased by ~ 5 MPa to maintain a zero displacement boundary, while the axial stress was increased by 50 MPa. It should be noted that if intergranular clay deformation, time-

dependent grain breakage and rearrangement were the mechanisms leading to time-dependent compaction in Slochteren sandstone under triaxial conditions, these should be (partly) inhibited in the zero lateral (uniaxial) strain experiments. So, while grains may experience stress corrosion cracking (see [*Hol et al.*, 2015a]), if this grain breakage does not lead to a (volumetric) strain due to the material being constrained from expanding laterally, grain rearrangement is limited and hence slip along grain boundaries is inhibited. Microstructural analysis will be performed in future to verify the deformation mechanism.

6.1.2 Slow stress-induced dissolution-precipitation in load-bearing grains

Though intergranular frictional slip and stress corrosion cracking are inferred to be the two mechanisms controlling sandstone compaction in the time period immediately after abandonment [*Hol et al.*, 2015a; *Pijnenburg et al.*, 2018; *Shinohara et al.*, in prep.], slow stress-induced dissolution-precipitation may play a role on the longer term. Stress-induced dissolution-precipitation, or Intergranular Pressure Solution (IPS), involves the dissolution of grain material at highly stressed grain contacts, followed by the diffusion and precipitation of this material to lower stressed grain boundaries [*Pluymakers and Spiers*, 2014; *Spiers et al.*, 2004]. The mechanism is dependent on grain contact stress, acting across asperities (roughness) in the grain boundary, and temperature. In quartz aggregates it operates faster at higher (effective) stress, porosity and temperature. However, once the contact stress becomes too low, such as due to porosity reduction, the process will stop and grain boundary healing will occur [*van Noort et al.*, 2008]. Under the pre-production stress conditions prevalent in the Groningen Gas Field, it was estimated that IPS would no longer be active, i.e. grain boundary healing had occurred, which would explain the preservation of porosity in the Slochteren sandstone despite its burial to 3 km depth.

Gas extraction effectively increased the stress acting across these healed grain boundaries, which suggests that over time the initialled healed contacts could experience a state of stress that would promote IPS again. The possibility of transient creep via dissolution of intergranular asperities between quartz grains (i.e. dissolution of grain boundary roughness) has not been evaluated yet. However, first order approximations, based on existing pressure models [*Pluymakers and Spiers*, 2014] and quartz dissolution kinetics [*Rimstidt*, 2015; *Tester et al.*, 1994], suggest that IPS creep rates could be on the order of 10^{-12}-10^{-13} s^{-1} for the current stress and porosity characteristics of the Groningen Gas Field [*Jefferd et al.*, in prep.]. These estimates are of the same order of magnitude as the current compaction rate of the field, i.e. ~0.2% strain in ~ 60 years (cf. Section 2) or an average compaction rate of ~10^{-12} s^{-1}. Furthermore, IPS in the Slochteren sandstone can be impacted by the presence of thin intergranular clay films [*Rutter and Elliott*, 1976], which could reduce diffusion rates of dissolved material through the grain boundary or enhance interface kinetics [*Greene et al.*, 2009; *Rutter and Elliott*, 1976]. Within the *DeepNL programme*, experiments are planned to quantify the effect of clay films on dissolution of grain boundary asperities.

6.2 Effect of pressure changes due to pressure equilibration and aquifer support

Once production is halted, the pore pressure in the field is expected to equilibrate over time, as currently the areas near the still-operational production wells are at a lower pore pressure than the more distal parts of the field. This means that the more northern parts of the field, currently at a higher pore pressure, will experience an increase in effective overburden stress with time. Likely pore pressure equilibration will be fairly rapid on the timescale of the lifetime of the field (e.g. see predictions for a scenario with continued minimum production [*Nederlandse Aardolie Maatschappij (NAM)*, 2021]). This suggests that the amount of compaction in those areas can be estimated following the deformation behaviour observed in previous experiments (cf. Figure 5 [*Pijnenburg et al.*, 2019a]), and possibly through use of DE models [*Mehranpour and Hangx*, in prep.-a; b; *Mehranpour et al.*, 2021]. It should be noted that the porosity in the northern part of the field is slightly lower than the central part, where the extensively tested Stedum-1 and Zeerijp-3A cores were obtained (12-16% vs. 18-22%; see Figure 1b). It has been shown that the stress-strain behaviour of the Slochteren sandstone is dependent on porosity, with less strain accumulating in lower porosity material [*Pijnenburg et al.*, 2018]. However, petrographical studies have demonstrated that there is an increase in grain-coating clay content towards the northern side of the field [*Visser*, 2016]. If this clay is present in more grain-to-grain contacts and/or of greater clay film thickness, it is possible that more strain can be accumulated than suggested by the current experiments [*Mehranpour and Hangx*, in prep.-b].

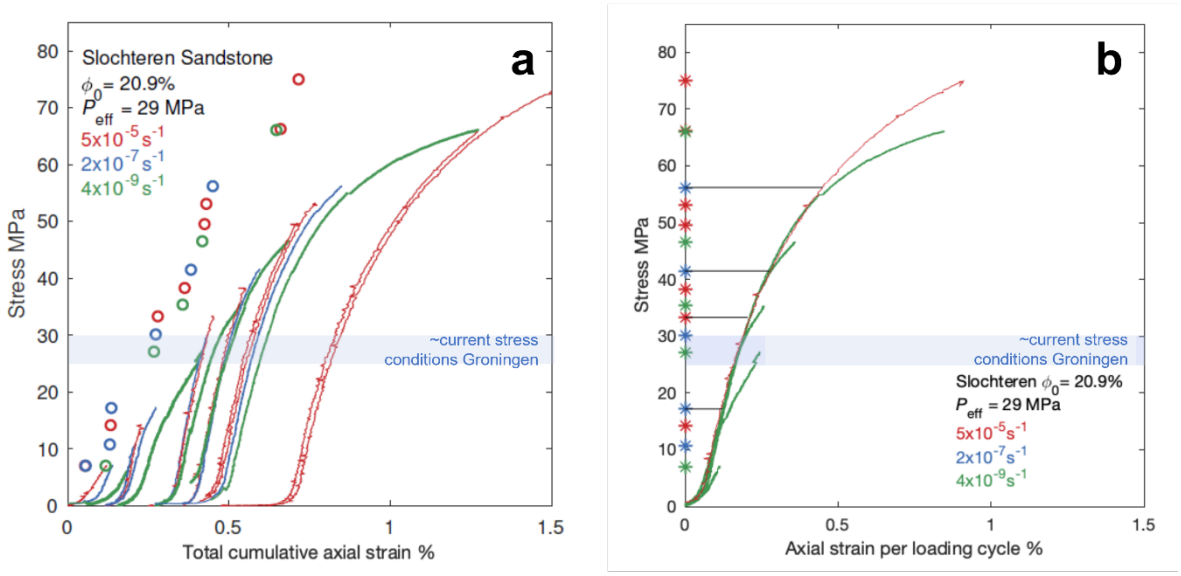

Figure 15. (a) Differential stress as a function of axial strain for Slochteren sandstone, deformed at Pceff = 29 MPa at 100°C. Each cycle of loading was carried out at one of three strain rates, and in between each cycle the sample was fully axially unloaded. The coloured circles correspond to the cumulative total inelastic strain generated at the end of each cycle. (b) Differential stress as a function of axial strain for a select number of cycles represented in (a). For all cycles, the previous inelastic strain has been removed to illustrate the effect of rate on the stress-strain behaviour. The stars correspond to the maximum stress reached in each cycle of the experiment and the black horizontal lines correspond to the maximum stress reached in the cycle prior to the slow loading cycles shown. Note, to improve readability the unloading curves are omitted from the figures (modified after Jefferd et al. [in prep.]).

On a longer timescale, the surrounding aquifers will be flowing into the reservoir leading to a pressure redistribution. Recent modelling predictions have suggested that this may lead to a substantial drop in pressure in the surrounding aquifers, while resulting in only little repressurisation of the Groningen Gas Field after abandonment [*Wildenborg et al.*, 2022]. Experiments under cyclic loading conditions at variable loading rates have demonstrated that the amount of inelastic, non-recoverable deformation increases at lower loading rates (Figure 15a). Furthermore, the cyclic loading experiments showed that cyclic loading only adds significantly more inelastic strain if the reloading rate is substantially lower than any previous cycle, or if a new higher stress value is reached and this effect is exacerbated when the new stress level is approached at a lower loading rate (Figure 15b). As larger amounts of time-dependent inelastic strains are produced as new stress levels are reached, it implies that the operating time-dependent deformation processes are highly stress-sensitive, such as is known for rate-dependent friction and stress corrosion cracking. On this basis it can be inferred that the amount of compaction in the surrounding aquifers depends on their mineralogy and porosity [*Mehranpour and Hangx*, in prep.-b] , and also on the rate at which the pore pressure decreases and how that rate compares to historical stresses and stressing rates. By contrast, the repressurisation of the Slochteren sandstone by only a few bars [*Wildenborg et al.*, 2022] will lead to only marginal recovery of elastic strain, as roughly 30-50% of the total strain obtained during the production stage is elastic (Section 5.1).

6.3 Preliminary model to describe time-dependent compaction by frictional slip and grain breakage

Experiments performed at loading rates down to 10^{-9} s^{-1} suggest that rate-dependent intergranular frictional slip plus subcritical (stress corrosion) crack growth and grain failure control rate-dependent deformation of the Slochteren sandstone. It should be noted that the rate of deformation depends on whether these processes can operate in series (i.e. sequentially, whereby the slowest controls the rate), or in parallel (i.e. concurrently, whereby the fastest controls the rate). In deforming granular materials, such as sandstones, serial or parallel operation of these mechanisms depends on i) the imposed mechanical boundary conditions (e.g. uniaxial compaction with zero lateral strain versus axial compression at fixed lateral stress) and ii) the microstructural state of the material, measured in terms of a suitable proxy, such as strain or porosity [*Jefferd et al.*, in prep.].

In conventional triaxial experiments, when a fully-consolidated or over-consolidated material is held at a constant lateral stress, both rate-dependent intergranular slip and subcritical grain failure can occur in parallel, with the faster mechanism controlling the deformation rate. However, under uniaxial strain conditions, such as

representative for in-situ conditions, the material is inhibited from deforming laterally. In that case, a fully- or over-consolidated material will not be able to deform by intergranular slip unless grain failure occurs, allowing for space for rearrangement. Now the slower, most resistive mechanism will control the deformation rate or rate-dependence. Similarly, microstructure plays an important role, particularly if the material is underconsolidated [*Pijnenburg et al.*, 2019a; b] when intergranular sliding motions may be possible without requiring grain breakage under both uniaxial and triaxial boundary conditions. Until a locked aggregate is achieved, which will be after only a small amount of strain under uniaxial conditions, rate-dependent intergranular slip and grain breakage by subcritical crack growth will operate in parallel, with the faster (easier) one dominating the rate-dependent deformation response. Once a locked aggregate is achieved, a switch in rate-controlling mechanism may occur, e.g. from easy intergranular slip at low strains to more difficult grain failure by subcritical cracking at higher strains (cf. 1-D creep experiments on Slochteren sandstone reported by [*Hol et al.*, 2015a; *Hol et al.*, 2018]) or vice-versa, and the material will respond as described for the consolidated case. This may explain why in the uniaxial experiments less deformation is achieved at the same applied axial stress.

The deformation behaviour resulting from rate-dependent intergranular slip has been described in a simplified microphysical model for axi-symmetric stress conditions [*Pijnenburg et al.*, 2018; 2019b]. The model is able to evaluate the role of rate-dependent frictional slip in controlling very small time-dependent deformations, such as observed during stress relaxation experiments [*Pijnenburg et al.*, 2018]. However, effects of strain on microstructure, and of microstructural heterogeneity on relating the shear and normal stresses on sliding grain contacts to the macroscopic (sample scale) stress state, are not considered. As a result, important effects, such as strain-dependent hardening and softening, are not captured and will need to be in future models.

To describe rate-dependent deformation controlled by subcritical crack growth, a preliminary model is being developed for grain failure by propagation of meridional cracks [*Jefferd et al.*, in prep.]. The choice for meridional cracks is warranted by the microstructural observations made in slow loading experiments on analogue sandstone (see also Section 6.1.1; [*Shinohara et al.*, in prep.]). This model is based on the original model of *Kendall* [1978] for meridional grain failure by equilibrium Griffith cracking, and will be extended to allow for kinetic growth at lower (subcritical), crack-tip stress intensities by the stress corrosion mechanism [*Atkinson*, 1984; *Lawn*, 1993]. It is assumed that subcritical Mode I (opening) cracks grow parallel to the maximum (vertical) compressive stress and open towards unloaded pore wall surfaces, i.e. they follow the path of least resistance in 3-D. In this case, crack growth (opening) is driven by the bending moment developed in the crack walls [*Kendall*, 1978] and will lead to a bulk axial strain increment, caused by local intergranular rearrangements and/or grain boundary clay film deformation occurring in response to grain splitting. Under 1-D strain conditions, this represents a volumetric strain increment, which is assumed to scale with grain volume. The associated strain rate is then obtained by calculating the grain lifetime, i.e. the time it takes for the crack to traverse the full length of the grain and lead to grain breakage. Therefore, it can be expected that axial strain rate directly reflects subcritical crack growth rate. Since in a real sandstone, there will be a distribution of grain diameters, the strain increment upon grain breakage and the energy release associated with that will also be distributed. As such, there will be a distribution of grain lifetimes and hence strain rate will evolve with time and strain/porosity reduction.

Through fitting to experimental data, such as stress-strain data obtained over a range of deformation rates at in-situ PT-stress-fluid conditions and using closely similar "sister" samples to minimize sample variability effects [e.g. *Shinohara and Hangx*, 2023; *Shinohara et al.*, in prep.], it is possible to obtain this evolving distribution. Suitable experimental approaches include monotonic loading tests, to minimise the effect of loading history [*Jefferd et al.*, in prep.]. When performed at decreasing loading rates, this should allow for separation and quantification of rate-independent and rate-dependent effects, while recognizing that time-dependent deformation may cause microstructural changes that in turn change the strain contribution by rate-independent deformation mechanisms. Combined with creep tests, rate-stepping tests and cyclic loading tests, it should be possible to obtain more systematic data linking deformation rate to effective stress and evolving strain or porosity. In addition, the deformation experiments could also include acoustic emission sensing to clarify the role of grain failure processes [*Brzesowsky et al.*, 2014], acoustic wave velocity measurements to constrain microcrack damage and/or changes in grain contact structure [*Hangx and Brantut*, 2019], optical/split-cylinder [*Pijnenburg et al.*, 2019b] and CT imaging during testing (provided sufficient resolution can be attained [*Van Stappen et al.*, 2022]), and the use of micro-dissolution marker methods [*Schutjens et al.*, 2021] to establish whether pressure solution may play any role in contributing to rate-dependent compaction under long-term field conditions.

7 Time-dependent deformation of the surrounding clay-rich formations

Though subsidence in the Groningen Gas Field is largely caused by reservoir compaction [*Doornhof et al.*, 2006], slow pore pressure equilibration of the over- and underlying, low permeability, clay-rich formations with the depleting reservoir [*Wildenborg et al.*, 2022] may lead to additional, time-dependent compaction [*Chang et al.*, 2014]. This is supported by in-situ compaction measurements, which have shown that the top of the underlying Carboniferous shales/siltstone and the overlying Ten Boer Member are also compacting, likely due to slow pressure equilibration with the reservoir [*Cannon and Kole*, 2017] (cf. Figure 2). These slow, time-dependent, vertical movements in the immediate under- and overburden formations will lead to further stressing of the many, steep (~75° dip) faults extending from the reservoir into the surrounding [*Kortekaas and Jaarsma*, 2017; *Nederlandse Aardolie Maatschappij (NAM)*, 2016]. Since no stress measurements have been performed below the reservoir, it is not known whether stresses on faults in the Carboniferous have decayed away since the last time they were active (Alpine inversion, 65-2.5 Ma [*de Jager and Visser*, 2017]), either by creep on the faults or through relaxation of the host rock between the faults [*Sone and Zoback*, 2014]. Additionally, varying rates of creep between the over-/underburden and the reservoir can transfer stress from weaker to stiffer parts of the system [*Buijze*, 2020], meaning that changes in production may lead to changes in the magnitude-frequency distribution of earthquakes (e.g. fewer but larger earthquakes).

The magnitude of stress relaxation since the Alpine inversion due to creep on faults penetrating into the Carboniferous was estimated to be minor compared to the estimated initial horizontal stress of ~200 MPa (i.e. ~5-10% reduction in horizontal stress, assuming a reverse fault scenario in line with Alpine inversion – see *Hunfeld and Spiers [2020 (unpublished)]*). If further tectonic loading after the Alpine inversion did not occur, relaxation of the horizontal stresses, at a constant vertical overburden stress, would slowly change the stress state from reverse to a state approaching normal faulting, though never reaching the critical state for (normal) reactivation, i.e. the horizontal stress is > 56 MPa. To relax away horizontal stresses ~200 MPa to nearly 56 MPa would require only ~0.3% creep strain. This implies that stress relaxation due to creep in the intact host rock surrounding the faults may play a much bigger role than creep on the fault in controlling the in-situ state of stress of the Carboniferous [*Sone and Zoback*, 2014]. Similar effects can be assumed for the thinner, overlying Ten Boer Member.

However, the mechanisms controlling time-dependent deformation (creep) in shales are not easily elucidated due to their complex interplay [*Rybacki et al.*, 2017]. Grain-scale mechanisms could range from deformation at constant volume (e.g. deformation of or along clay- or organic matter-rich constituents [*Rassouli and Zoback*, 2018; *Rybacki et al.*, 2017]) to compaction of porosity (e.g. open pores, but also porous organic matter and mineral assemblages [*Chang and Zoback*, 2009; *Geng et al.*, 2018; *Rassouli and Zoback*, 2018; *Rybacki et al.*, 2017]), stress corrosion cracking [*Geng et al.*, 2018; *Rassouli and Zoback*, 2018; *Rybacki et al.*, 2017] and pressure solution [*Geng et al.*, 2018]. Furthermore, slow dewatering (e.g. in response to pore pressure changes [*Chang et al.*, 2014]), as well as pressure-induced desorption of fluid (water, methane, CO_2 [*Liu et al.*, 2017; *M Zhang et al.*, 2018]), could also play in important role, as the rate of compaction by dewatering/desorption is controlled by the rate at which the fluid can diffuse out of the rock [*Chang et al.*, 2014; *Liu et al.*, 2017]. From studies on shales, it has become evident that the mechanical strength and creep behaviour of shales are strongly controlled by their mineralogy, specifically the clay and/or organic matter content [*Sone and Zoback*, 2014]. Furthermore, the influence of the highly laminated nature of both the Ten Boer claystone and the Carboniferous shales/siltstones cannot be neglected in determining their creep behaviour (Figure 16). Within the *DeepNL programme*, the mechanisms leading to creep in these clay-rich formations, and the link to the petrophysical properties of the formations, are currently being investigated.

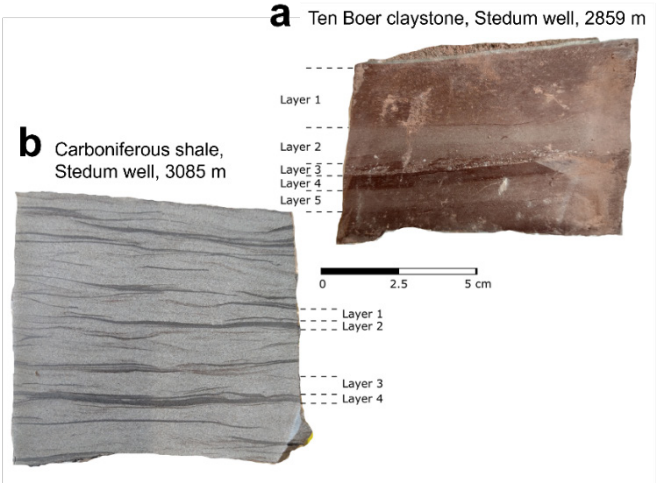

Figure 16. Hand specimens of (a) the Ten Boer claystone overburden and (b) the Carboniferous shale underburden, obtained from the Stedum-1 well. As can be noted, both clay-rich rocks show clear laminations, with likely mm-scale variations in mineralogy. Currently detailed analyses are being performed to identify and quantify the mineral content of the laminations observed in both rocks.

8 Implications of time-dependent compaction in the reservoir and surroundings for production-related seismicity

From the above it can be concluded that experiments performed on Slochteren sandstone, simulating stress changes during production of the Groningen Gas Field, show that the bulk of compaction develops near-instantaneously, i.e. over time-scales of hours-days [*Hol et al.*, 2018; *Pijnenburg et al.*, 2018; *Shinohara and Hangx*, 2023]. Slower experiments (at strain rates down to 10^{-9} s^{-1}) performed over weeks show decelerating creep deformation, contributing a modest 10-20% to the inelastic strain accumulated during active loading [*Jefferd et al.*, in prep.; *Pijnenburg et al.*, 2018; *Shinohara and Hangx*, 2023].

Overall, the present experimental and mechanistic constraints presented in Sections 5 and 6 suggest a modest time-dependence, or rate-sensitivity, of compaction of the Groningen gas reservoir sandstone. This is in line with long-term (months) uniaxial strain creep experiments performed on similar sandstones from a nearby field (i.e. from a Wadden Sea gas field, located within several tens of km from the Groningen field) [for details see the extensive report by *Hol et al.*, 2015b]. These experiments showed that at similar stress conditions (σ_1^{eff} = 77 MPa, σ_3^{eff} = 23 MPa, (σ_1 – σ_3) = 54 MPa) to those relevant to Groningen, the axial strain rate decreased with time, reaching values below 10^{-11} s^{-1} after one to three months. The axial strains developing over the experiment duration ranged between 0.05 and 0.10%, and contributed a modest 10 to 20% relative to the near-instantaneous inelastic strains that had developed during active loading [*Hol et al.*, 2015a; *Hol et al.*, 2015b], i.e. similar to the time-dependent contributions of 10-20% reported in Chapters 5 and 6.

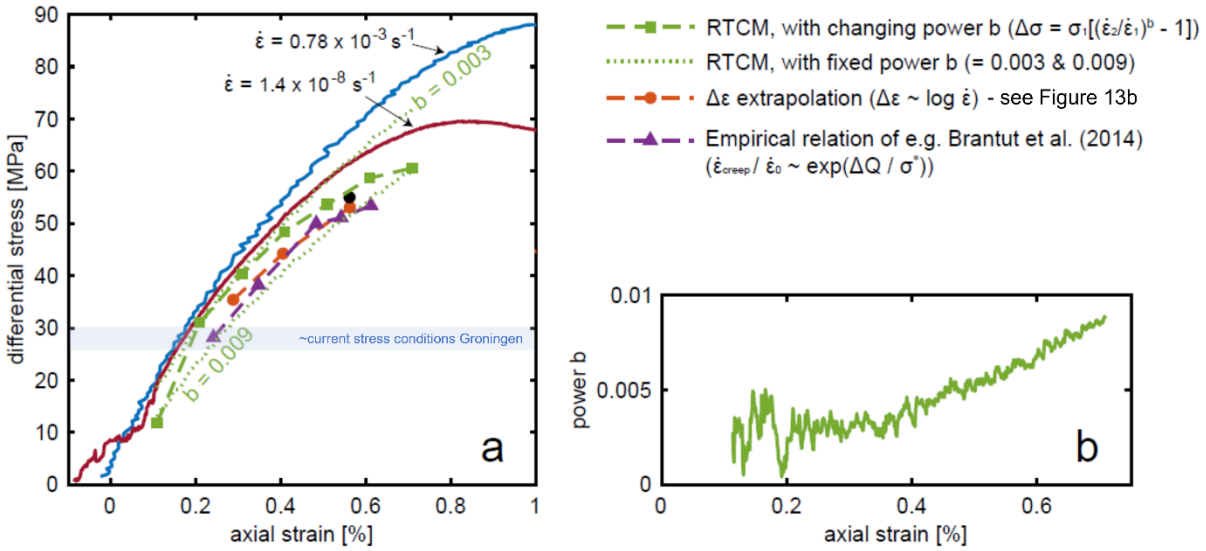

Figure 17. (a) Empirically-constrained extrapolated stress-strain curves and their peak stress. Extrapolation of the lab data obtained by Shinohara et al. [in prep.] on Bleurswiller sandstone at strain rates of 10^{-3} (blue curve) and 10^{-8} s^{-1} (red curve) to field strain rate of 10^{-12} s^{-1}. The extrapolated stress-strain curves were obtained by fitting different time-dependent models to the experimental data. These models include the Rate Type Compaction Model (RTCM) with changing power b as a function of axial strain, as shown in (b) (dashed green curve), the RTCM model with a fixed power b of 0.003 and 0.009 (dotted green curves), an empirical linear-log extrapolation of Δε vs. axial strain rate data (see Figure 13b; dashed orange curve) and the empirical relation proposed by Brantut et al. [2014] (dashed purple curve). Figure modified after Shinohara et al. [in prep.].

The implication is that compaction models developed for time-independent deformation [*Pijnenburg and Spiers*, 2020; *Pijnenburg et al.*, 2019a], or time-dependent deformation (e.g. the RTCM [*de Waal*, 1986; *de Waal and Smits*, 1988] or RTiCM models [*Pruiksma et al.*, 2015]), calibrated to experimental data obtained over hours-weeks can adequately approximate the compaction behaviour at vertical strain rates down to 10^{-9} s^{-1}, and likely even down to 10^{-11} s^{-1}. Indeed, the presently observed trends are qualitatively similar to those captured in the RTCM and RTiCM models [*de Waal*, 1986; *Pruiksma et al.*, 2015], which are frequently used to model reservoir compaction and associated subsidence. If we use the data obtained in the systematic experiments performed on the Bleurswiller sandstone, which showed similar mechanical behaviour as the Slochteren sandstone, extrapolation to field strain rates of 10^{-12} s^{-1} suggests that additional strains of 10-50% can be expected (i.e. inelastic strain in excess of what has already been accumulated at deformation rates of up to 10^{-8}-10^{-9} s^{-1}; see Figure 17). This broad range in forecasted compaction illustrates the need to better constrain the models used for extrapolation to field

timescales. In order to enhance the applicability of these various models at strain rates relevant to (post-)production of the Groningen gas field ($\dot{\varepsilon} < 10^{-12}$ s^{-1}) and time scales (decades) which cannot be accessed in the lab, understanding the processes underlying our experimental data is required. However, based on the experimental work to date, notable the experiments reaching strain rates only one order of magnitude faster than the current field compaction rate, suggest that the expected inelastic strain after abandonment will likely be at the lower end of this forecasted range.

The work presented here suggests that during production, compaction is dominated by processes that are (virtually) rate-insensitive, like poro-elastic deformation, and intergranular clay compaction and slip. The virtually instantaneous deformation accommodated by these intergranular mechanisms suggests that the modest, time-dependent strains developing during long-term (weeks-months) creep experiments may be governed by a different mechanism, notably by stress corrosion (intragranular) cracking [*Hol et al.*, 2015a; *Pijnenburg et al.*, 2019a; *Shinohara et al.*, in prep.]. However, the additional inelastic strain due to (inferred) stress corrosion cracking [*Hol et al.*, 2015a; *Shinohara and Hangx*, 2023; *Shinohara et al.*, in prep.], relative to that accumulated instantaneously during loading, was found to be small (10-20%), particularly under uniaxial strain conditions and even while exploring strain rates down to 10^{-11} s^{-1} (see Section 6.1.1). To what extent long-term (decades-centuries) compaction behaviour will be influenced by this slow creep process, or by other creep processes (e.g. pressure solution; cf. Section 6.1.2) still requires further investigation and quantification.

In summary, the present experimental and mechanistic constraints suggest that reservoir compaction in the Groningen Gas Field is largely rate-insensitive, with only a modest contribution of time- or rate-sensitive mechanisms. To date, the compaction rate has been predominantly governed by the production rate (compaction strain governed by total depletion), while any ongoing compaction due to stress-corrosion cracking, or other slow creep processes beyond the currently planned field closure, is expected to be modest. This inference is consistent with microstructural investigation of undepleted (SDM-1) and depleted (ZRP-3A) reservoir sandstones from the Groningen field, which showed no detectable evidence that pressure solution, nor intragranular cracking contributed to compaction during more than 50 years of production [*Verberne et al.*, 2020]. Developments in Discrete Element Methods models make it possible to predict the rate-insensitive compaction accurately [*Mehranpour and Hangx*, in prep.-a; b; *Mehranpour et al.*, 2021], and can hence be used to evaluate reservoir compaction in different locations on the field due to pressure equilibration or repressurisation, with rate-sensitive mechanisms aimed to be added at a later stage.

Despite this, even if the Slochteren reservoir formation does not exhibit much ongoing compaction after field closure due to time-dependent compaction processes, that does not necessarily imply independence of subsidence and seismicity from production rate and strategy. Even if reservoir compaction is fully time-independent, subsidence and seismicity may be influenced by time-dependent (creep) deformation of the overlying Basal Zechstein and rock salt [*Marketos et al.*, 2016], and by pore pressure re-equilibration within/near the reservoir (e.g. the clay-rich Ten Boer and Ameland members; see Section 7), and/or the underlying low-permeable (Carboniferous) shales (Section 7). In addition, time dependent behaviour may perhaps be caused by transient fluid flow along faults [*Zbinden et al.*, 2017].

9 References

† Research performed in the context of the *NAM-funded research programme*.
‡ Research performed in the context of the *DeepNL research programme*.

Amthor, J. E., and J. Okkerman (1998), Influence of Early Diagenesis on Reservoir Quality of Rotliegende Sandstones, Northern Netherlands1, *AAPG Bull.*, *82*(12), 2246-2265, doi:10.1306/00aa7f04-1730-11d7-8645000102c1865d.

Atkinson, B. K. (1984), Subcritical crack growth in geological materials, *Journal of Geophysical Research*, *89*(B6), 4077-4114.

Baud, P., E. Klein, and T.-f. Wong (2004), Compaction localization in porous sandstones: spatial evolution of damage and acoustic emission activity, *Journal of Structural Geology*, *26*(4), 603-624, doi:http://dx.doi.org/10.1016/j.jsg.2003.09.002.

Baud, P., T. Reuschlé, Y. Ji, C. S. N. Cheung, and T.-f. Wong (2015), Mechanical compaction and strain localization in Bleurswiller sandstone, *Journal of Geophysical Research: Solid Earth*, n/a-n/a, doi:10.1002/2015JB012192.

Bernabé, Y., D. T. Fryer, and R. M. Shively (1994), Experimental Observations of the Elastic and Inelastic Behaviour of Porous Sandstones, *Geophysical Journal International*, *117*(2), 403-418, doi:https://doi.org/10.1111/j.1365-246X.1994.tb03940.x.

Bourne, S. J., S. J. Oates, J. van Elk, and D. Doornhof (2014), A seismological model for earthquakes induced by fluid extraction from a subsurface reservoir, *Journal of Geophysical Research: Solid Earth*, *119*(12), 8991-9015, doi:https://doi.org/10.1002/2014JB011663.

Brantut, N., M. J. Heap, P. Baud, and P. G. Meredith (2014), Rate- and strain-dependent brittle deformation of rocks, *Journal of Geophysical Research: Solid Earth*, *119*(3), 1818-1836, doi:10.1002/2013JB010448.

Breckels, I. M., and H. A. M. van Eekelen (1982), Relationship Between Horizontal Stress and Depth in Sedimentary Basins, *Journal of Petroleum Technology*, *34*(09), 2191-2199, doi:10.2118/10336-pa.

Brown, K. M., et al. (2017), The action of water films at Å-scales in the Earth: Implications for the Nankai subduction system, *Earth and Planetary Science Letters*, *463*, 266-276, doi:https://doi.org/10.1016/j.epsl.2016.12.042.

Brzesowsky, R. H., S. J. T. Hangx, N. Brantut, and C. J. Spiers (2014), Compaction creep of sands due to time-dependent grain failure: Effects of chemical environment, applied stress, and grain size, *Journal of Geophysical Research: Solid Earth*, *119*(10), 7521-7541, doi:10.1002/2014JB011277.

† Buijze, L. (2020), Numerical and experimental simulation of fault reactivation and earthquake rupture applied to induced seismicity in the Groningen gas field, PhD thesis, 304 pp, Utrecht University, Utrecht, The Netherlands.

Buijze, L., P. Van den Bogert, B. Wassing, B. Orlic, and J. Ten Veen (2017), Fault reactivation mechanisms and dynamic rupture modelling of depletion-induced seismic events in a Rotliegend gas reservoir, *Netherlands Journal of Geosciences*, *96*(5), S131-S148, doi:10.1017/njg.2017.27.

Cannon, M., and P. Kole (2017), The First Year of Distributed Strain Sensing (DSS) Monitoring in the Groningen Gas Field, *Unrestricted Rep. SR.17.00934*, 73 pp.

Chang, C., E. Mallman, and M. Zoback (2014), Time-dependent subsidence associated with drainage-induced compaction in Gulf of Mexico shales bounding a severely depleted gas reservoir, *AAPG Bulletin*, *98*(6), 1145-1159, doi:10.1306/11111313009.

Chang, C., and M. D. Zoback (2009), Viscous creep in room-dried unconsolidated Gulf of Mexico shale (I): Experimental results, *Journal of Petroleum Science and Engineering*, *69*(3), 239-246, doi:https://doi.org/10.1016/j.petrol.2009.08.018.

† Cuesta Cano, A., J. F. Van Stappen, T. K. T. Wolterbeek, and S. J. T. Hangx (2021), Uniaxial compaction of sand using 4D X-ray tomography: The effect of mineralogy on grain-scale compaction mechanisms, *Materials Today Communications*, *26*, 101881, doi:https://doi.org/10.1016/j.mtcomm.2020.101881.

David, E. C., N. Brantut, A. Schubnel, and R. W. Zimmerman (2012), Sliding crack model for nonlinearity and hysteresis in the uniaxial stress–strain curve of rock, *International Journal of Rock Mechanics and Mining Sciences*, *52*, 9-17, doi:https://doi.org/10.1016/j.ijrmms.2012.02.001.

de Jager, J., and C. Visser (2017), Geology of the Groningen field – an overview, *Netherlands Journal of Geosciences*, *96*(5), s3-s15, doi:10.1017/njg.2017.22.

de Waal, J. A. (1986), On the rate type compaction behaviour of sandstone reservoir rock, [s.n.], [S.l.].

de Waal, J. A., and R. M. M. Smits (1988), Prediction of Reservoir Compaction and Surface Subsidence: Field Application of a New Model, *SPE Formation Evaluation*, *3*(02), 347-356, doi:10.2118/14214-pa.

Dempsey, D., and J. Suckale (2017), Physics-based forecasting of induced seismicity at Groningen gas field, the Netherlands, *Geophysical Research Letters*, *44*(15), 7773-7782, doi:https://doi.org/10.1002/2017GL073878.

Doornhof, D., T. G. Kristiansen, N. B. Nagel, P. D. Patillo, and C. Sayers (2006), Compaction and subsidence, *Oilfield Review*, *Autumn 2006*, 50-68.

Fortin, J., A. Schubnel, and Y. Guéguen (2005), Elastic wave velocities and permeability evolution during compaction of Bleurswiller sandstone, *International Journal of Rock Mechanics and Mining Sciences*, *42*(7–8), 873-889, doi:http://dx.doi.org/10.1016/j.ijrmms.2005.05.002.

Gaupp, R., A. Matter, J. D. Platt, K. Ramseyer, and J. Walzebuck (1993), Diagenesis and Fluid Evolution of Deeply Buried Permian (Rotliegende) Gas Reservoirs, Northwest Germany, *AAPG Bulletin*, *77*, 1111-1128.

Gaupp, R., and J. A. Okkerman (2011), Diagenesis and Reservoir Quality of Rotliegend Sandstones in the Northern Netherlands—A Review, in *The Permian Rotliegend of the Netherlands*, edited by J. Grötsch and R. Gaupp, pp. 193-228, SEPM Society for Sedimentary Geology, doi:10.2110/pec.11.98.0193.

Geng, Z., A. Bonnelye, M. Chen, Y. Jin, P. Dick, C. David, X. Fang, and A. Schubnel (2018), Time and Temperature Dependent Creep in Tournemire Shale, *Journal of Geophysical Research: Solid Earth*, *123*(11), 9658-9675, doi:https://doi.org/10.1029/2018JB016169.

Greene, G. W., K. Kristiansen, E. E. Meyer, J. R. Boles, and J. N. Israelachvili (2009), Role of electrochemical reactions in pressure solution, *Geochimica et Cosmochimica Acta*, *73*(10), 2862-2874, doi:https://doi.org/10.1016/j.gca.2009.02.012.

Grötsch, J., A. Sluijk, K. V. Ojik, M. D. Keijzer, J. Graaf, and J. Steenbrink (2011), The Groningen Gas Field: Fifty Years of Exploration and Gas Production From a Permian Dryland Reservoir, in *The Permian Rotliegend of the Netherlands*, edited by J. Grötsch and R. Gaupp, pp. 11-36, SEPM Society for Sedimentary Geology, doi:10.2110/pec.11.98.0011.

Hangx, S. J. T., and N. Brantut (2019), Micromechanics of High-Pressure Compaction in Granular Quartz Aggregates, *Journal of Geophysical Research: Solid Earth*, *124*(7), 6560-6580, doi:10.1029/2018jb016494.

Hangx, S. J. T., C. J. Spiers, and C. J. Peach (2010), Creep of simulated reservoir sands and coupled chemical-mechanical effects of CO_2 injection, *Journal of Geophysical Research*, *115*, B09205, doi:10.1029/2009JB006939.

Hettema, M. H. H., P. M. T. M. Schutjens, B. J. M. Verboom, and H. J. Gussinklo (2000), Production-Induced Compaction of a Sandstone Reservoir: The Strong Influence of Stress Path, *SPE-65410-PA*, doi:10.2118/65410-PA.

Hol, S., A. P. Mossop, A. J. van der Linden, P. M. M. Zuiderwijk, and A. H. Makurat (2015a), Long-term compaction behavior of Permian sandstones - An investigation into the mechanisms of subsidence in the Dutch Wadden Sea, edited, American Rock Mechanics Association.

Hol, S., A. van der Linden, S. Bierman, F. Marcelis, and A. H. Makurat (2018), Rock Physical Controls on Production-induced Compaction in the Groningen Field, *Scientific Reports*, *8*(1), 7156, doi:10.1038/s41598-018-25455-z.

Hol, S., A. J. van der Linden, P. M. M. Zuiderwijk, F. H. M. Marcelis, and A. H. Coorn (2015b), Mechanical characterization of Permian reservoir sandstone from the Moddergat-3 well in the Dutch Wadden Area, *Unrestricted Rep. SR.15.11614*, 48 pp.

† Hunfeld, L. B., and C. J. Spiers (2020 (unpublished)), Horizontal stress in the Carboniferous substrate, edited, p. 6.

† Jefferd, M. A., S. J. T. Hangx, and C. J. Spiers (in prep.), The effect of loading rate and loading history on deformation of the reservoir sandstone of the Groningen Gas Field.

Kendall, K. (1978), The impossibility of comminuting small particles by compression, *Nature*, *272*(5655), 710-711, doi:10.1038/272710a0.

Ketelaar, G., W. van der Veen, and D. Doornhof (2011), Monitoring effecten van bodemdaling op Ameland-Oost, *Unrestricted Rep.*, 21 pp.

Kortekaas, M., and B. Jaarsma (2017), Improved definition of faults in the Groningen field using seismic attributes, *Netherlands Journal of Geosciences*, *96*(5), s71-s85, doi:10.1017/njg.2017.24.

Lawn, B. R. (1993), *Fracture of solids*, 2nd ed., Cambridge University Press.

Lele, S. P., S.-Y. Hsu, J. L. Garzon, N. DeDontney, K. H. Searles, G. A. Gist, P. F. Sanz, E. A. Biediger, and B. A. Dale (2016), Geomechanical Modeling to Evaluate Production-Induced Seismicity at Groningen Field, paper presented at Abu Dhabi International Petroleum Exhibition & Conference.

Liu, J., P. A. Fokker, and C. J. Spiers (2017), Coupling of swelling, internal stress evolution, and diffusion in coal matrix material during exposure to methane, *Journal of Geophysical Research: Solid Earth*, *122*(2), 844-865, doi:https://doi.org/10.1002/2016JB013322.

Marketos, G., and M. D. Bolton (2009), Compaction bands simulated in Discrete Element Models, *Journal of Structural Geology*, *31*(5), 479-490, doi:https://doi.org/10.1016/j.jsg.2009.03.002.

Marketos, G., C. J. Spiers, and R. Govers (2016), Impact of rock salt creep law choice on subsidence calculations for hydrocarbon reservoirs overlain by evaporite caprocks, *Journal of Geophysical Research: Solid Earth*, *121*(6), 4249-4267, doi:https://doi.org/10.1002/2016JB012892.

‡ Mehranpour, M. H., and S. J. T. Hangx (in prep.-a), How Uncertainty in 3D In-Situ Stress Affects Reservoir Compaction Behavior: A DEM Case Study of the Groningen Gas Field.

‡ Mehranpour, M. H., and S. J. T. Hangx (in prep.-b), Insight into the Mechanical Behavior of Groningen Sandstone Using Discrete Element Method: Grain Size Distribution and Mineralogy Effects.

† Mehranpour, M. H., S. J. T. Hangx, and C. J. Spiers (2021), Compaction of the Groningen Gas Reservoir Sandstone: Discrete Element Modeling Using Microphysically Based Grain-Scale Interaction Laws, *Journal of Geophysical Research: Solid Earth*, *126*(9), e2021JB021722, doi:https://doi.org/10.1029/2021JB021722.

Nederlandse Aardolie Maatschappij (NAM) (2013), Technical Addendum to the Winningsplan Groningen 2013: Subsidence, Induced Earthquakes and Seismic Hazard Analysis in the Groningen Field, *Unrestricted Rep.*, 243 pp.

Nederlandse Aardolie Maatschappij (NAM) (2016), Technical Addendum to the Winningsplan Groningen 2016: Production, Subsidence, Induced Earthquakes and Seismic Hazard and Risk Assessment in the Groningen Field., *Unrestricted Rep.*, 163 pp.

Nederlandse Aardolie Maatschappij (NAM) (2019), Review and update of: Study and Data Acquisition Plan Induced Seismicity in Groningen Including Addendum and Review by Regulator (SodM), *Unrestricted Rep.*, 231 pp.

Nederlandse Aardolie Maatschappij (NAM) (2021), Reservoir Pressure and Subsidence Groningen Field: update for Production Profile GTS - raming 2021*Rep.*, 46 pp.

† Pijnenburg, R. P. J. (2019), Deformation Behavior of Reservoir Sandstones from the Seismogenic Groningen Gas Field: An experimental and mechanistic study, PhD thesis, 293 pp, Utrecht University, Utrecht.

† Pijnenburg, R. P. J., and C. J. Spiers (2020), Microphysics of Inelastic Deformation in Reservoir Sandstones from the Seismogenic Center of the Groningen Gas Field, *Rock Mechanics and Rock Engineering*, doi:10.1007/s00603-020-02215-y.

† Pijnenburg, R. P. J., B. A. Verberne, S. J. T. Hangx, and C. J. Spiers (2018), Deformation Behavior of Sandstones From the Seismogenic Groningen Gas Field: Role of Inelastic Versus Elastic Mechanisms, *Journal of Geophysical Research: Solid Earth*, *123*(7), 5532-5558, doi:10.1029/2018jb015673.

† Pijnenburg, R. P. J., B. A. Verberne, S. J. T. Hangx, and C. J. Spiers (2019a), Inelastic Deformation of the Slochteren Sandstone: Stress-Strain Relations and Implications for Induced Seismicity in the Groningen Gas Field, *Journal of Geophysical Research: Solid Earth*, *124*(5), 5254-5282, doi:10.1029/2019jb017366.

† Pijnenburg, R. P. J., B. A. Verberne, S. J. T. Hangx, and C. J. Spiers (2019b), Intergranular Clay Films Control Inelastic Deformation in the Groningen Gas Reservoir: Evidence From Split-Cylinder Deformation Tests, *Journal of Geophysical Research: Solid Earth*, *124*(12), 12679-12702, doi:10.1029/2019jb018702.

Pluymakers, A. M. H., and C. J. Spiers (2014), Compaction creep of simulated anhydrite fault gouge by pressure solution: theory v. experiments and implications for fault sealing in *Rock Deformation from Field, Experiments and Theory: A Volume in Honour of Ernie Rutter*, edited by D. R. Faulkner, E. Mariani and J. Mecklenburgh, Geological Society of London Special Publications, London, doi:http://dx.doi.org/10.1144/SP409.6.

Potyondy, D. O., and P. A. Cundall (2004), A bonded-particle model for rock, *International Journal of Rock Mechanics and Mining Sciences*, *41*(8), 1329-1364, doi:https://doi.org/10.1016/j.ijrmms.2004.09.011.

Pruiksma, J. P., J. N. Breunese, K. van Thienen-Visser, and J. A. de Waal (2015), Isotach formulation of the rate type compaction model for sandstone, *International Journal of Rock Mechanics and Mining Sciences*, *78*, 127-132, doi:https://doi.org/10.1016/j.ijrmms.2015.06.002.

Rassouli, F. S., and M. D. Zoback (2018), Comparison of Short-Term and Long-Term Creep Experiments in Shales and Carbonates from Unconventional Gas Reservoirs, *Rock Mechanics and Rock Engineering*, *51*(7), 1995-2014, doi:10.1007/s00603-018-1444-y.

Rimstidt, J. D. (2015), Rate equations for sodium catalyzed quartz dissolution, *Geochimica et Cosmochimica Acta*, *167*, 195-204, doi:https://doi.org/10.1016/j.gca.2015.07.030.

Rutter, E. H., and D. Elliott (1976), The Kinetics of Rock Deformation by Pressure Solution [and Discussion], *Philosophical Transactions of the Royal Society of London. Series A, Mathematical and Physical Sciences*, *283*(1312), 203-219.

Rybacki, E., J. Herrmann, R. Wirth, and G. Dresen (2017), Creep of Posidonia Shale at Elevated Pressure and Temperature, *Rock Mechanics and Rock Engineering*, *50*(12), 3121-3140, doi:10.1007/s00603-017-1295-y.

Schutjens, P. M., T. W. Fens, and R. M. M. Smits (1995), Experimental observations of the uniaxial compaction of quartz rich reservoir rock at stresses up to 80 MPa, paper presented at The 5th International Symposium on Land Subsidence, Balkema, Rotterdam.

Schutjens, P. M., C. J. Spiers, and A. R. Niemeijer (2021), Surface microstructures developed on polished quartz crystals embedded in wet quartz sand compacted under hydrothermal conditions, *Scientific Reports*, *11*(1), 14920, doi:10.1038/s41598-021-94376-1.

‡ Shinohara, T., and S. Hangx (2023), Inelastic strain due to slow deformation of clay-bearing porous sandstone, in *84th EAGE Annual Conference & Exhibition*, edited, pp. 1-5, European Association of Geoscientists and Engineers, Vienna, Austria, doi:https://doi.org/10.3997/2214-4609.202310957.

‡ Shinohara, T., S. J. T. Hangx, and C. J. Spiers (in prep.), The effect of loading rate on the deformation behavior of highly porous sandstones.

Smith, J. D., J.-P. Avouac, R. S. White, A. Copley, A. Gualandi, and S. Bourne (2019), Reconciling the Long-Term Relationship Between Reservoir Pore Pressure Depletion and Compaction in the Groningen Region, *Journal of Geophysical Research: Solid Earth*, *124*(6), 6165-6178, doi:https://doi.org/10.1029/2018JB016801.

Sone, H., and M. D. Zoback (2014), Time-dependent deformation of shale gas reservoir rocks and its long-term effect on the in situ state of stress, *International Journal of Rock Mechanics and Mining Sciences*, *69*, 120-132, doi:https://doi.org/10.1016/j.ijrmms.2014.04.002.

Spiers, C. J., S. De Meer, A. R. Niemeijer, and X. Zhang (2004), Kinetics of rock deformation by pressure solution and the role of thin aqueous films, in *Physicochemistry of water in geological and biological systems*, edited by S. Nakashima, C. J. Spiers, L. Mercury, P. A. Fenter and J. M. F. Hochella, pp. 129-158, Universal Academy Press, Inc., Tokyo, Japan.

† Spiers, C. J., S. J. T. Hangx, and A. R. Niemeijer (2017), New approaches in experimental research on rock and fault behaviour in the Groningen gas field, *Netherlands Journal of Geosciences*, *96*(5), s55-s69, doi:10.1017/njg.2017.32.

Tembe, S., P. Baud, and T.-f. Wong (2008), Stress conditions for the propagation of discrete compaction bands in porous sandstone, *Journal of Geophysical Research: Solid Earth*, *113*(B9), B09409, doi:10.1029/2007JB005439.

Tester, J. W., W. G. Worley, B. A. Robinson, C. O. Grigsby, and J. L. Feerer (1994), Correlating quartz dissolution kinetics in pure water from 25 to 625°C, *Geochimica et Cosmochimica Acta*, *58*(11), 2407-2420, doi:https://doi.org/10.1016/0016-7037(94)90020-5.

Van Eijs, R. M. H. E. (2015), Neotectonic stresses in the permian Slochteren formation of the Groningen field, *Unrestricted Rep. EP201510210531*, 33 pp, NAM.

Van Eijs, R. M. H. E., F. M. M. Mulders, M. Nepveu, C. J. Kenter, and B. C. Scheffers (2006), Correlation between hydrocarbon reservoir properties and induced seismicity in the Netherlands, *Engineering Geology*, *84*(3), 99-111, doi:https://doi.org/10.1016/j.enggeo.2006.01.002.

van Noort, R., H. J. M. Visser, and C. J. Spiers (2008), Influence of grain boundary structure on dissolution controlled pressure solution and retarding effects of grain boundary healing, *Journal of Geophysical Research: Solid Earth*, *113*(B3), B03201, doi:10.1029/2007JB005223.

† Van Stappen, J., J. A. McBeck, B. Cordonnier, R. P. J. Pijnenburg, F. Renard, C. J. Spiers, and S. J. T. Hangx (2022), 4D Synchrotron X-ray Imaging of Grain Scale Deformation Mechanisms in a Seismogenic Gas Reservoir Sandstone During Axial Compaction, *Rock Mechanics and Rock Engineering*, *55*(8), 4697-4715, doi:10.1007/s00603-022-02842-7.

† Verberne, B. A., S. J. T. Hangx, R. P. J. Pijnenburg, M. F. Hamers, M. R. Drury, and C. J. Spiers (2020), Drill core from seismically active sandstone gas reservoir yields clues to internal deformation mechanisms, *Geology*, *49*(5), 483-487, doi:10.1130/g48243.1.

† Verberne, B. A., and C. J. Spiers (2017), A Quantitative Microstructural Investigation of Depleted and Undepleted Reservoir Sandstones, in *51st U.S. Rock Mechanics/Geomechanics Symposium*, edited, American Rock Mechanics Association, San Francisco, California, USA.

Visser, C. (2016), Petrographic Aspects of the Rotliegend of the Groningen field: Inventory and quick-look analysis of petrographic data from the Groningen field, *Unrestricted Rep.*, 36 pp.

Visser, C., R. Porter, and J. Solano Viota (2016), On the implementation of Sedimentological data in Porosity Modelling for the Groningen field, *Unrestricted Rep. EP201609201569*, 55 pp.

Waldmann, S. (2012), Geological and mineralogical investigation of Rotliegend gas reservoirs in the Netherlands and their potential for CO_2 storage, PhD thesis, 252 pp.

Waldmann, S., A. Busch, K. van Ojik, and R. Gaupp (2014), Importance of mineral surface areas in Rotliegend sandstones for modeling CO2–water–rock interactions, *Chemical Geology*, *378-379*, 89-109, doi:https://doi.org/10.1016/j.chemgeo.2014.03.014.

† Waldmann, S., and R. Gaupp (2016), Grain-rimming kaolinite in Permian Rotliegend reservoir rocks, *Sedimentary Geology*, *335*, 17-33, doi:https://doi.org/10.1016/j.sedgeo.2016.01.016.

Waldmann, S., B. A. Verberne, and C. J. Spiers (2017), Physical mechanisms and mechanics governing compaction of the Slochteren sandstone: Progress report on the potential impact of the shifting GWC on water-rock interactions, *Confidential Rep. work performed within Research Agreement UI49358*, 29 pp, Utrecht University.

Walsh, J. B. (1965), The effect of cracks on the compressibility of rock, *Journal of Geophysical Research*, *70*(2), 381-389.

Wassing, B. B. T., L. Buijze, and B. Orlic (2016), Modelling of Fault Reactivation and Fault Slip in Producing Gas Fields Using a Slip-weakening Friction Law, paper presented at 50th U.S. Rock Mechanics/Geomechanics Symposium.

Wildenborg, T., L. Peters, A. Moghadam, P. Fokker, K. Geel, S. Nelskamp, S. Bottero, A. Wiersma, and A. Marsman (2022), KEM-19 - Evaluation of post-abandonment fluid migration and ground motion risks in subsurface exploitation operations in the Netherlands, *Public Rep. KEM 19/202003118*, 161 pp.

Wong, T.-f., P. Baud, and E. Klein (2001), Localized failure modes in a compactant porous rock, *Geophysical Research Letters*, *28*(13), 2521-2524, doi:10.1029/2001GL012960.

Wu, X. Y., P. Baud, and T.-f. Wong (2000), Micromechanics of compressive failure and spatial evolution of anisotropic damage in Darley Dale sandstone, *International Journal of Rock Mechanics and Mining Sciences*, *37*(1), 143-160, doi:https://doi.org/10.1016/S1365-1609(99)00093-3.

Zbinden, D., A. P. Rinaldi, L. Urpi, and S. Wiemer (2017), On the physics-based processes behind production-induced seismicity in natural gas fields, *Journal of Geophysical Research: Solid Earth*, *122*(5), 3792-3812, doi:https://doi.org/10.1002/2017JB014003.

Zhang, J., T.-F. Wong, and D. M. Davis (1990), Micromechanics of pressure-induced grain crushing in porous rocks, *Journal of Geophysical Research*, *95*(B1), 341-352.

Zhang, M., S. M. de Jong, C. J. Spiers, A. Busch, and H. M. Wentinck (2018), Swelling stress development in confined smectite clays through exposure to CO_2, *International Journal of Greenhouse Gas Control*, *74*, 49-61, doi:https://doi.org/10.1016/j.ijggc.2018.04.014.